The Start-up Phase of ASDEX Tokamak

D.B.Albert

IPP III/54 January 1980

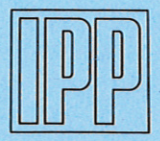

MAX-PLANCK-INSTITUT FÜR PLASMAPHYSIK

8046 GARCHING BEI MÜNCHEN

MAX-PLANCK-INSTITUT FÜR PLASMAPHYSIK

GARCHING BEI MÜNCHEN

The Start-up Phase of ASDEX Tokamak

D.B.Albert

IPP III/54 January 1980

Die nachstehende Arbeit wurde im Rahmen des Vertrages zwischen dem Max-Planck-Institut für Plasmaphysik und der Europäischen Atomgemeinschaft über die Zusammenarbeit auf dem Gebiete der Plasmaphysik durchgeführt.

IPP III/54 D.B. Albert The Start-up Phase of ASDEX Tokamak

Abstract

Investigations of the start-up phase in a large tokamak are made using a zero-dimensional, time-dependent model which describes the ionization of the neutral gas in terms of coupled mass and energy conservation equations for five components - H_2^o, H_2^+, H_1^o, H_1^+ and electrons. These equations are coupled to an equivalent external OH cricuit of the tokamak and the plasma behaviour during start-up for various discharge conditions and models for loss mechanisms has been studied. A simple model for the effect of transverse magnetic fields on the discharge formation has also been included to investigate the effect of a divertor field and also magnetic limiter operation.

Introduction

The process of discharge formation in a tokamak becomes increasingly more important to the overall performance as the dimensions of the plasma are increased. As well as being an important factor in the design of the poloidal field system, the start-up phase also has a strong influence on the development of density and current profiles and the influx of impurities into the plasma. A detailed understanding of the plasma behaviour during this phase is therefore essential for determination of operating parameters which will ensure successful and efficient initiation of the discharge.

In previous investigations of the start-up process in a tokamak /1-5/, various models for the ionization of the neutral gas have been developed and the influence of parameters such as initial filling pressure, low-Z impurity concentration, loop voltage and pre-ionization studied in some detail. Because comparatively little is known about the complex transport processes occurring during this period of transition between neutral gas and plasma /6/, such investigations have been constrained to zero-dimensional treatments. In a large tokamak with a complicated poloidal field structure such as ASDEX /7/, the details of this transport could be expected to play a more important role in determining the dynamics of the start-up phase.

An attempt to take account of the two-dimensional nature of the discharge development in ASDEX tokamak is presented in the following with the intention of providing a model which can be used to explain experimental results as well as to determine optimal conditions for discharge initiation. In consideration of this work, some general observations concerning the important aspects of this phase of tokamak operation are also presented.

Description of Model

During the process of ionization of the neutral gas by the induced electric field, the behaviour of the partially ionized plasma in the magnetic field of the tokamak will correspond to a complex and time dependent mixture of single particle and macroscopic effects. Since the behaviour during this early phase of plasma formation would be dominated by collisional atomic and molecular interactions, a bulk description of the components provides a reasonable model of the behaviour. By modifying this zero-dimensional treatment with an approximation to the two-dimensional effects, it is then possible to treat the problem without the complexity and many uncertain assumptions of a fully two-dimensional model.

The plasma behaviour is described in terms of the temperatures and densities of five components; H_2^o, H_1^o, H_2^+, H_1^+ and electrons. In a manner similar to that used in modelling the ohmic heating process in the C-stellarator/8/ and in ORMAK /4/, three different regions of the plasma are distinguished: (see Figure 1)

V_o - the plasma volume = $2\pi R\pi r_o^2$

available to the components e, H_1^+, H_1^o. (R is the major radius)

V_1 - volume of discharge chamber = $2\pi R\pi r_1^2$

and

V_2 - volume available to e, H_1^+, H_1^o, H_2^+ = $2\pi R\pi(r_o^2-r_2^2)$.

Here r_2 is the radius within which no H_2^o or H_2^+ components are found and is determined by

$$r_2 = \begin{cases} r_o - \lambda_{H_2^o} & \text{for } r_o > \lambda_{H_2^o} \\ 0 & r_o < \lambda_{H_2^o} \end{cases}$$

where $\lambda_{H_2^o}$ is the mean free path of a H_2 molecule with respect to ionization or dissociation - i.e. the distance that a H_2^o molecule, which is approximately at the wall temperature can penetrate into the plasma without undergoing reaction

$$\lambda_{H_2^o} = \frac{\nu_{H_2}}{3n_e \left(\sum S_{ion} + \sum S_{diss} \right)}$$

S_{ion} and S_{diss} are ionization and dissociation rate coefficients respectively and ν_{H_2} is the H_2^o thermal velocity. Thus the volume available to molecular hydrogen will be $V_1 - V_o + V_2$.

The various ionization, dissociation, recombination and charge exchange reactions between the components which have been considered are given in Table I. The collisional excitation of atomic hydrogen is included only as an energy loss for electrons and no detailed treatment of the distribution of these excited states has been attempted. In addition, a facility for investigating various models for recycling processes at the plasma boundary was included by supposing that H_1^+ leaving the plasma can recombine and return as H_1^o with a probability ψ_1 and as H_2^o with probability Φ 1. Similary H_2^+ can recombine to form H_1^o with probability ψ_2 and H_2^o with probability Φ_2.

A number of mechanisms for charged particle loss from the plasma have been considered in order to determine the effect of the various processes on the start-up. The total loss rate which was assumed to be uniform over the cross-section, is given by the sum of:

Bohm loss: $R_B = \frac{T_e\ (eV)}{16\ r_o^2\ B_T\ (T)}$

Pseudo classical: $R_{PC} = \frac{5 \cdot 10^{-9}\ n_e\ Z_{eff}}{I_p^2 \sqrt{T_e\ (kV)}}$

Curvature and gradient losses (single particle): $R_C = \frac{m}{eB_T R} \left(\frac{V_\perp^2}{2} + V_d^2\right)$

where Vd is the drift velocity and $V_\perp$ is a transverse velocity which was assumed to be the thermal velocity so $\frac{mV_\perp^2}{2} = \frac{3}{2} kT_e$

Stray field loss: particles that follow a field line of strength B_V which is normal to the main toroidal field B_T, are lost at a rate

$$R_V = \frac{V_d}{r_o} \frac{B_V}{B_T}$$

Mass and energy conservation equations for each of the plasma components may thus be written to describe the processes discussed above as well as additional energy transfer mechanisms such as charged particle energy equilibration, bremsstrahlung, ohmic heating and energy losses associated with oxygen impurities (the complete set of equations is given in detail in Appendix A). Closure of these equations is accomplished by determining the evolution of the plasma current from a model for the external circuit, which describes the manner in which the currents in the OH circuit are related to the plasma current. From the model given in Fig. 2, we determine the primary current I_p from the circuit equations

$$V_{loop} = \frac{-MdI_1}{dt} = R_p I_p + \frac{d}{dt}(L_p I_p)$$

and

$$\frac{-MdI_p}{dt} = (R_V + R_1)\ I_1 + L_1 \frac{dI_1}{dt}$$

$$L_p = \mu_o R \left[\ln \frac{8R}{a} - 2 + \frac{\ell i}{2} \right]$$

is the plasma inductance and $\frac{\mu_o \ell i}{4\pi}$ = plasma internal inductance/unit length.

R_p the plasma resistance is calculated from

$$R_p = \frac{2R}{r_o^2}\eta \qquad \eta = \eta_{sp} + \eta_{neut}$$

the resistivity due to neutral collisions was determined from the relation /4/

$$\eta_{neut} = 5.04 \times 10^{-6} \frac{n_{H_2 o}}{ne} \Omega m$$

while $\eta_{sp} = 3.26 \times 10^{-9} Z_{eff} \beta \ln \Lambda \, Te^{-3/2} \Omega m$

where $\ln \Lambda$ is the coulomb logarithm

$$\beta = \frac{0.457}{1.077 + Z_{eff}} + 0.29 \quad (T_e \text{ in keV})$$

The ohmic heating circuit in ASDEX is operated by driving an initial current I_1 (o) in the OH coils and then closing the switch to the discharge resistor R_v at time t_o to produce a high voltage for breakdown.

An important aspect of modelling the start-up phase is the time interval between application of the toroidal electric field and confinement of the plasma by its own magnetic field. During this period plasma particles are lost rapidly because of curvature effects as well as losses due to transverse fields. In the case of a poloidal divertor configuration, the balance between these losses and the rotational transform of the plasma current is particularly important and will be con-

sidered in more detail later.

During this pre-confinement phase, the electron drift velocity may be determined from the empirical formula /3/

$$V_d = 35\ E/p_o \text{ m/s}$$

where E is the electric field in v/m and

p_o is the neutral gas filling pressure in Torr.

For typical ASDEX parameters, the curvature loss rate, R_C is much smaller than the loss rate, R_V due to a transverse magnetic field B_V of only 1 gauss so this will be the dominant loss. We may model the transition to self-confinement of the plasma by considering that this loss is present only until the poloidal field of the current exceeds the field B_V. In this manner it will be possible to determine the degree of pre-ionization required to reduce this pre-confinement period to a minimum.

Start-up Characteristics

Using the model for the start-up process described above, the effect of variation of parameters corresponding to initial conditions of the discharge has been investigated with the dimensions and external circuit configuration of the ASDEX experiment. An example of the behaviour of the quantities in this model is given in Figure 3. A characteristic feature of the start-up process is the time taken to convert the neutral gas completely into ionized particles. During this time, the electron temperature is constant because energy gained from the electric field by the electrons is lost in ionization of neutrals and the electron temperature cannot rise until this process is completed. The duration of this period is determined by the quantity of gas to be ionized, the applied electric field, as well as the loss rate of electron energy and it is

the interrelation between these quantities which determines the efficiency of the start-up process. By varying these parameters in the model, it is possible to determine the nature of their influence on the start-up process and we may similarly derive values for unknown quantities, such as recycling rates, which provide the best fit to experimental results.

An important result of the variation in the behaviour of the model with changes in the applied electric field is illustrated in Figure 4. Here it may be seen that although the breakdown time decreases with increasing OH transformer voltage, the flux required for breakdown exhibits a minimum. Because the amount of volt seconds consumed during start-up provides a measure of the efficiency of this process, it is desirable to have some knowledge of the location of this minimum and the manner in which its position varies with the parameters of the model. Although an investigation of the behaviour for all of the possible combinations of the parameters would not be feasible or meaningful without some comparison with experiment, some useful observations of tendencies in the parameter variations may be made.

Investigation of the various loss mechanisms included in the model has indicated that the Bohm, pseudo-classical and drift losses have relatively little influence on the time required for breakdwon, indicating that the "diffusive" rate of these processes is considerably slower than the characteristic ionization rates of the gas breakdown. An order of magnitude increase in the Bohm loss, for example, results in an increase in the breakdown time of less than 2 %, however, the discharge behaviour following completion of ionization is markedly different, exhibiting a slower temperature rise and a more rapid decay in electron density. The stray field loss model described previously has a significantly stronger influence on the duration of the ionization phase because the characteristic time scale of the free-streaming of particles along field lines that leave the plasma region is inherently

faster than the diffusive losses. Although the self-confining field of the plasma current can cancel the stray field loss quickly enough for it to have little effect on the breakdown time (as for the case of $R_V = 0.3\Omega$ in Figure 5), a critical situation can occur where a rapid rise in the time required for breakdown with small increases in the stray field is observed. This is the case for the curve corresponding to $R_V = 0.2\Omega$ in Figure 5. While it may be considered sufficient to raise the applied voltage above the level at which this occurs, significant increases in the flux consumption then result, as illustrated by the increase in the minimum volt-sec for a stray field of 40 G in Figure 4. This point will be considered in more detail later in this report where the effects of divertor fields are modelled.

Initial Gas Fill

The filling density of neutral gas in the vessel is not determined strictly by the desired electron density in the discharge, because gas may be added after the initial breakdown has occurred and the electron temperature has begun to increase. As indicated in the results of calculations shown in Figure 6, a sharp increase in the breakdown time with small increases in the initial density can occur at low loop voltage and we can observe that the location of the minimum in volt-sec consumption will also vary with initial filling density. Although these calculations indicate that the shortest breakdown time will occur at the lowest filling pressure, a lower limit will be set by the occurrence of runaway electrons which can quickly carry large amounts of the input energy out of the plasma. In addition, a lower starting density requires more gas to be injected to reach a specific electron density and this could consume more flux than the static fill method.

The process of electron runaway during start-up has been recognized as playing an important role in determining breakdown dynamics as well as the early influx of impurities /9/. A time lag between the application of the electric field and the appearance of a detectable electron density has been observed under some experimental conditions /10/ and has been explained in terms of the time required for the runaway electrons to be confined by the magnetic field of the plasma current /6/. Theoretical calculations of the runaway rate in a partially ionized plasma /11/ have found little agreement with experiment /12/ because of the very complicated nature of the neutral gas effect and the observed influence of impurities on their behaviour. These uncertainties, together with the problems of large variations in the electron and neutral densities across the plasma profile, and the difficulties of determining trajectories in complicated field configurations , make the prediction of the influence of runaways a very difficult problem. The question of runaway effects during start-up therefore remains an area where more detailed experimental investigation is necessary.

A simple model of the runaway process predicts in agreement with experimental results,the qualitative result that runaway production is reduced by decreasing the electric field or increasing the electron density. With all other conditions constant, we should therefore expect a reduction in the appearance of runaways with an increase in the degree of preionization of the neutral gas.

The influence of increasing the preionization rate may be seen in the results of Figure 7. With the total number of particles held constant, the time required for breakdown decreases in accordance with the increase in the number of charged particles produced by the preionization. There is an additional effect in the presence of a stray field loss, because the point at

which the current can confine itself is reached more quickly when the initial preionization is increased as shown by the results for B_v = 40 G in Figure 7. This point emphasizes the need for good preionization which becomes more important in larger devices where the costs of such techniques as microwave start-up /13/ may be outweighed by the reduction in costs of the OH system required.

Effect of the Divertor Field on Start-up

In a tokamak with a poloidal divertor configuration, the transverse magnetic field has a null along the axis of symmetry of the minor cross-section but away from this axis the field strength increases to a value which could produce large losses of particles during the start-up phase. As demonstrated previously, the presence of such transverse field losses can significantly increase the time required for breakdown so that a good understanding of the influence of the divertor field on the start-up process is necessary for a more complete model of this phase.

The losses associated with particles following field lines of the divertor which leave the plasma region will be balanced by the effect of the self-confining field of the plasma current. In order to derive a quantitative assessment of the nature of this balance during the plasma formation phase, a method for determining an effective loss rate factor for the magnetic configuration was developed. Beginning with the assumption that plasma particles move along field lines transverse to the main toroidal field B_T , with a velocity $V_f = V_d \frac{Bv}{B_T}$ we can determine that the time required for such a particle to leave the plasma region is $T = \int \frac{dl}{v_f}$ where the integral is taken along a field line from the starting point until it leaves the plasma. The corresponding loss rate is R = 1/T and this may then be averaged over the cross-section, taking a zero loss

for particles which are confined and therefore return to their starting point.

Thus $\bar{R} = \left\langle \frac{1}{T} \right\rangle = \frac{V_d}{B_T} \left\langle \frac{1}{\int \frac{dl}{B_v}} \right\rangle$

is the average loss rate from which we may calculate an equivalent loss magnetic field $B_{eq} = \frac{B_T r_o \bar{R}}{V_d}$

Using the magnetic field calculated from the positions of the divertor field coils in ASDEX, the equivalent loss field was determined by dividing the plasma region into a grid and evaluating the above integrals along field lines starting from each grid section. The self field of the plasma current was modelled by a single toroidal filament at the plasma centre resulting in field configurations such as that given in Figure 8. Further refinements of the model were made, such as the inclusion of a parabolic density profile so that the loss rates were weighted by the density at the starting point and conversion to a parabolic current distribution. Calculating the magnetic field of the plasma current at a particular point by considering the current inside this radius to be concentrated at the plasma centre, however, leads to a considerable error in this model. Because the field calculation is toroidal, the region of closed field lines associated with the current reach the outside of the torus before the inside is reached, so that the calculated average loss ratio does not decrease to zero for full current. It would therefore be necessary to use the magnetic field determined from a full equilibrium calculation in order to make the results of this model more realistic.

Because the self-magnetic field of the plasma current produces a zone of confinement that results in two distinct regions of the plasma, it is more appropriate to take account of this dis-

tinction than to average the losses over the whole cross-section within the limiter of the discharge chamber. In the inner confined region, losses will be mainly of a diffusive nature although there will still be some drifts associated with fields which are non-zero on the minor cross-section symmetry axis. These drifts will however be significantly reduced by the presence of a rotational transform. Within the region where the particles travelling along transverse field lines cannot be confined by the field of the plasma current, it is appropriate to determine the effective loss rate using the method described above. Since, however, such a treatment would require a further subdivision of the plasma region to deal with the temperatures and densities in each zone separately, it has been considered sufficient to treat the border of the confinement region as the plasma boundary. For the purposes of a zero-dimensional treatment this approximation is quite good because particles outside the confinement zone are lost at a much faster rate than those within this plasma boundary.

In order to examine the effect of such a variable boundary on the start-up process, a description of the manner in which the size of the containment region varies with the magnitude of the plasma current is necessary. This calculation may be done using a free boundary equilibrium code which determines the location of the separatrix for various values of the plasma current. Results of such calculations for various coil configurations including that of ASDEX, illustrated in Figure 9 display a power law characteristic of the form

$$\frac{A}{Am} = \left(\frac{I}{I_m}\right)^{\gamma}$$

where I_m is the full plasma current and A_m is the corresponding cross-sectional area. This "magnetic limiter" behaviour may thus be included in the start-up calculations by determining the plasma radius at any time from the above formula using the corresponding value of the plasma current.

For conditions the same as those used for the results in Figure 3, the start-up calculations were made with the inclusion of the expanding current channel effects described above. The results shown in Figure 10 indicate that although some of the neutral gas was ionized, there was no current rise and the dischage extinguished. An explanation for this can be found in the time variation of the loop voltages, since it can be seen here that the resistive voltage rises above the total loop voltage resulting in a negative inductive component of the voltage and thus a decreasing current. The resistive voltage rises as the plasma current increases so that in order to maintain the current rise, it is necessary for the resistance to decrease due an expansion of the plasma radius. If the expansion of the current channel occurs at a faster rate then the discharge formation continues as illustrated in Figure 11 where the exponent in the relation between the plasma area and the current has been reduced. It is also possible to overcome this barrier associated with the rate of confinement region expansion by increasing the loop voltage (see Figure 12).

For the case of a moving plasma boundary it may also be observed that the time dependence of the electron density exhibits a rapid rise to a large peak followed by a slower decay. This behaviour demonstrates a form of 'pumping' of the confinement region which occurs as neutrals are ionized and trapped. As the source of neutrals becomes exhausted and the radius of the plasma increases further, the density decreases to the values which would be produced in a full-radius start-up.

The results described above indicate the importance of the moving plasma boundary description to the energy balance during start-up. It has also been observed that the increase in flux consumption associated with the presence of the divertor field should not lead to serious reductions in the OH flux available for the main discharge and these effects should probably be offset by the improvement in plasma purity due to the magnetic limiter operation.

It has been assumed in the model discussed so far that the plasma begins as a small but finite filament of current that forms in the neighbourhood of the null in the divertor field on the symmetry axis. This simple theoretical model will be complicated in practice by the influence of small misalignments of coil structures as well as time dependent eddy currents induced in the vacuum vessel components and also the poloidal field coils. Minimization of the time required for the current to confine itself is therefore more a question of experimental adjustments of stray fields within the discharge region. For this reason, the question of how and where the discharge begins to form remains to be investigated in detail.

Gas Puffing and Impurities

A facility for simulation of neutral gas injection into the discharge after it has been initiated was also included in the model in order to study the effects of gas puffing on the start-up. An example of the results obtained under such conditions is given in Figure 13, which corresponds to the same parameters as in Figure 3 except that half of the neutral gas is injected at a constant rate over a period of 5 ms beginning 1 ms after the start of the discharge. Comparing these results with those of the static fill case, one observes that the temperature increase, which can be correlated with the depletion of the neutral hydrogen atoms, occurs at a considerably earlier time. There is also a corresponding reduction in the resistive voltage component resulting in a faster rate of current rise even though the electron density requires much more time to reach its final value. Such a faster rate of current rise would lead to improved confinement during the critical stage of the discharge when the current channel is being formed. This effect would therefore be particularly important improving the start-up efficiency in the presence of a divertor field. Although

these results indicate that start-up with a low filling pressure followed by gas puffing to increase the density to the desired level can offer some important advantages over purely static filling, these effects must be weighed against the increase in runaway production which occurs at lower filling densities.

The rate at which neutral gas will flow into the discharge during the start-up will in practice be determined by such complex processes as trapping and release of the gas in the vessel walls /14/ and the mechanism of neutral penetration into the plasma. It would however,be possible to obtain a reasonable understanding of this process by adjusting such parameters as the effective vessel volume, neutral recycling coefficients and flow rates in the model to fit experimental results.

In a manner similar to the 'pumping' effect of neutrals discussed previously, low-Z impurities may also be concentrated in the discharge column as it is forming /15/ and the radiation losses due to these effects have been shown to be capable of having a very significant effect on the energy balance during the start-up /1/. In order to include a description of these losses in the model, a calculation of the time dependent evolution of oxygen ionization states and the associated ionization and radiation losses has been coupled to the plasma model (see Appendix B for a description of this treatment). An illustration of the effect of 1 % oxygen impurities on the start-up is given in Figure 14 for the same discharge conditions as in Figure 3. The increased losses due to the impurities produce only a small increase in the time required for ionization of the neutral gas but the main effect is seen as a significant reduction in the rate of temperature rise following the ionization. The influence of the impurity is small when the temperature is of the order of 5 eV as only the first ionization state can be produced. Losses increase rapidly with temperature, however, once this limit is exceeded and the energy loss due to

the impurities becomes of the same order as the ohmic power input resulting in a significant retardation of the current rise and increase of the plasma resistance.

Conclusions

Calculations made using the model of the start-up phase of a tokamak described in this report, have demonstrated a number of significant features of this process which should be important to producing efficient initiation of the discharge. In particular the attempt at inclusion of two-dimensional effects in the model has demonstrated the importance of the balance between losses due to particle motion along transverse magnetic fields and the self-confining field of the plasma current. These results indicate the need for a more detailed understanding of the manner in which the individual particle motions begin to act collectively and form a confined current region. Experimental investigations of this point coupled with development of the description of this phase which is used in the model would be necessary for a more accurate prediction of this behaviour.

It has also been observed that the applied loop voltage can be selected to minimize the flux consumed during breakdown, for a particular set of initial conditions. However, other effects of the loop voltage variation, such as the influence on runaway electron production, must also be considered when choosing the operating conditions. Since the occurence of electron runaway also depends on the initial neutral density as well as the degree of pre-ionization in a manner which is not yet well understood, this question remains as a subject where detailed experimental investigation is required. Such information would be necessary in order to determine the best compromise between lowering the initial filling density to reduce required loop voltage and thus the flux consumption, and the deleterious

effects of an increased runaway component.

Since this model was developed with the intention of initially investigating the important features of the start-up process and to subsequently be developed interactively with experimental observations, no extensive investigation of the broad range of parameters available in the model has been attempted. With the additional information obtained from fitting the model behaviour to experimental results, more reliable prediction of the optimal conditions for discharge formation and in particular magnetic limiter behaviour, should be possible.

Acknowledgements

The author wishes to express his appreciation for the information provided by S.E.Attenberger of ORNL concerning the start-up model developed by himself and F.B.Marcus. He would also like to thank Dr.K.Lackner for his advice and assistance as well as the results of his equilibrium calculations of magnetic limiter configurations.

Density and Temperature Evolution Equations

Rate equations for the density of each of the five components of the plasma considered in the model may be determined from the reaction equations given in Table I, with the addition of loss and recycling terms. Since the volumes of the different regions of the plasma are also time-dependent, the equations are derived by considering the conservation of total particle numbers.

The variables used in the equations are defined as follows:

n_{10} - density of neutral hydrogen atoms, H_1^o

n_{20} - density of neutral hydrogen molecules H_2^o

n_{1+} - density of protons, H_1^+

n_{2+} - density of molecular ions, H_2^+

n_e - electron density

$$n_{eo} = n_{1+} + \frac{V_2}{V_o} n_{2+} \quad \text{in } V_o$$

$$n_{e2} = n_{1+} + n_{2+} \quad \text{in } V_2$$

τ = particle loss time; $\frac{1}{\tau}$ is the loss rate

$$\frac{d}{dt}(V_o n_{1+}) = V_o n_{eo} n_{10} S_1 + V_2 n_{e2} n_{20} S_3 + 2V_2 n_{e2} n_{20} S_5 + V_2 n_{e2} n_{2+} S_6 - V_2 n_{1+} n_{20} S_8 - \frac{V_o n_{1+}}{\tau}$$

$$\frac{d}{dt}(V_2 n_{2+}) = V_2 n_{e2} n_{20} S_2 + V_2 n_{1+} n_{20} S_8 - V_2 n_{e2} n_{2+} S_6 - V_2 n_{e2} n_{2+} S_{10} - \frac{V_2 n_{2+}}{\tau}$$

$$\frac{d}{dt}(V_1 n_{10}) = - V_o n_{eo} n_{10} S_1 + V_2 n_{e2} n_{20} S_3 + 2V_2 n_{e2} n_{20} S_4 + V_2 n_{e2} n_{2+} S_6 + V_2 n_{1+} n_{2+} S_8 + 2V_2 n_{e2} n_{2+} S_{10} + V_o \frac{n_{1+}}{\tau} \psi_1 + \frac{2V_2 n_{2+} \psi 2}{\tau}$$

$$\frac{d}{dt}((V_1-V_o+V_2)n_{2o}) = - V_2 n_{e2} n_{2o} S_2 - V_2 n_{e2} n_{2o} S_3 - V_2 n_{e2} n_{2o} S_4 - V_2 n_{e2} n_{2o} S_5 - V_2 n_{1+} n_{2o} S_8 + V_o \frac{n_{1+}\phi_1}{2\tau} + \frac{V_2 n_{2+}\phi_2}{\tau}$$

The energy conservation equations may be determined in a similar manner to describe the temperatures of the various components using the following variable definitions:

T_e - electron temperature in keV

T_{1+} - proton temperature in keV

T_{2+} - molecular ion temperature in keV

T_{1o} - neutral atomic hydrogen temperature in keV

T_{2o} - neutral melecular hydrogen temperature in keV

The densities are described in units of m^{-3}.

For the electron energy, the equation is as follows

$$\frac{d}{dt}(V_o \frac{3}{2} n_{eo} T_e) = P_{OH} - V_o n_{eo} n_{1o} S_1 E_1 - V_2 n_{e2} n_{2o} S_2 E_2 - V_2 n_{e2} n_{2o} S_3 E_3 - V_2 n_{e2} n_{2o} S_4 E_4 - V_2 n_{e2} n_{2o} S_5 E_5 - V_2 n_{e2} n_{2+} S_6 E_6 - V_o n_{eo} n_{1o} S_{2x} (1.08\ E_{L_\alpha}) - V_o n_{eo} n_{1o} S_{3x} (.65\ E_{L\beta} + .52\ E_{H_\alpha}) - V_o n_{eo} n_{1o} S_{4x} (.51\ E_{L_\gamma} + .33\ E_{H\beta}) - V_2 n_{e2} n_{2+} S_{10} \frac{3}{2} T_e - V_o \frac{3}{2} \frac{T_e}{\tau}(n_{1+} + n_{2+}) - V_2 n_{e2} n_{2o} (S_2+S_3+S_4+S_5) E_{2o} - P_{BR} - P_{ei} - P_{imp}$$

where P_{OH} is the ohmic heating rate = $\frac{V_o}{10^3 e} \eta \left[\frac{I_p}{\pi r_o^2}\right]^2$

e is the electron charge

P_{imp} is the impurity loss rate (described in Appendix B)

P_{BR} is the Bremsstrahlung loss rate = $3.3 \cdot 10^{-21}\ V_o Z_{eff} n_{eo}^2 \sqrt{T_e}$

P_{ei} is the electron-ion equilibration rate

$$P_{ei} = P_{ei1} + P_{ei2}$$

$$P_{ei1} = 1.53 \cdot 10^{-19} V_o n_{eo} n_{1+} (T_e - T_{1+}) \frac{\ell n \Lambda}{A_{1+} T_e^{3/2}}$$

$$P_{ei2} = 7.7 \cdot 10^{-20} V_2 n_{e2} n_{2+} (T_e - T_{2+}) \frac{\ell n \Lambda}{A_{2+} T_e^{3/2}}$$

determined from the couloumb energy transfer rate caculated from the formula

$$P_{10} = \frac{\sqrt{2\pi}}{4\pi^2 \epsilon_o^2} \frac{n_1 n_o}{m_1 m_o} e^4 \frac{(kT_1 - kT_o) \ell n \Lambda}{\left[\frac{kT_1}{m_1} + \frac{kT_o}{m_o}\right]^{3/2}}$$

The energy losses due to excitation of neutral hydrogen atoms were determined from the photon emission rate for various excited states estimated from experiments on the C-Stellarator /16,4/

using $E_{H_\alpha} = 1.89$ eV $\quad E_{H_\beta} = 2.55$ eV

$E_{L_\alpha} = 10.2$ eV $\quad E_{L\beta} = 12.09$ eV $\quad E_{L_\gamma} = 12.75$ eV

An estimate for the energy loss associated with excitation of molecular hydrogen, E_{20} was also made from these experiments as

$E_{20} \sim (1.44\ T_e)$ eV for $T_e < 5$ eV

and ~ 7.2 eV above 5 eV

For the ion and neutral energies the following equations can be similarly derived

$$\frac{d}{dt}(V_o \tfrac{3}{2} n_{1+} T_{1+}) = V_2 n_{e2} n_{20} S_3 \frac{(\frac{3}{2} T_{20} + \Delta E_3)}{2} + V_2 n_{e2} n_{20} S_5 (\tfrac{3}{2} T_{20} + \Delta E_5) + V_2 n_{e2} n_{2+} S_6 \frac{(\frac{3}{2} T_{2+} + \Delta E_6)}{2} + P_{ei1} - P_{ii} - V_o \tfrac{3}{2} \frac{n_{1+} T_{1+}}{\tau}$$

$$+ V_o n_{eo} n_{10} S_1 \frac{3}{2} T_{10} - V_o n_{1+} n_{10} S_7 \frac{3}{2} (T_{1+} - T_{10})$$
$$- V_2 n_{1+} n_{20} S_8 \frac{3}{2} T_{1+}$$

H_2^+ energy equation:

$$\frac{d}{dt}(V_2 \frac{3}{2} n_{2+} T_{2+}) = V_2 n_{e2} n_{20} S_2 \frac{3}{2} T_{20} - V_2 n_{e2} n_{2+} S_6 \frac{3}{2} T_{2+}$$
$$+ V_2 n_{1+} n_{20} S_8 \frac{3}{2} T_{20} + V_2 n_{2+} n_{20} S_9 \frac{3}{2} (T_{20} - T_{2+})$$
$$+ P_{ii} + P_{ei2} - V_2 n_{e2} n_{2+} S_{10} \frac{3}{2} T_{2+} - V_2 \frac{3}{2} \frac{n_{2+} T_{2+}}{\tau}$$

where P_{ii} is the ion-ion equilibration term

$$P_{ii} = 3.3 \cdot 10^{-18} n_{1+} n_{2+} \frac{(T_{1+} - T_{2+})}{(T_{1+} + \frac{T_{2+}}{2})^{3/2}} \frac{\ell n \Lambda}{\sqrt{A_{2+}}}$$

where A_{1+}, A_{2+} are the atomic numbers of the ions.

H_{10} energy equation:

$$\frac{d}{dt}(\frac{3}{2} V_o n_{10} T_{10}) = - V_o n_{eo} n_{10} S_1 \frac{3}{2} T_{10} + V_2 n_{e2} n_{20} S_3 \frac{(\frac{3}{2} T_{20} + \Delta E_3)}{2}$$
$$+ V_2 n_{e2} n_{20} S_4 (\frac{3}{2} T_{20} + \Delta E_4)$$
$$+ V_2 n_{e2} n_{2+} S_6 \frac{(\frac{3}{2} T_{2+} + \Delta E_6)}{2}$$
$$+ V_o n_{1+} n_{10} S_7 \frac{3}{2} (T_{1+} - T_{10}) + V_2 n_{1+} n_{20} S_8 \frac{3}{2} T_{1+}$$
$$+ V_o n_{1+} \psi_1 \frac{3}{2} T_w + V_2 \frac{n_{2+}}{\tau} 2\psi_2 \frac{3}{2} T_w$$
$$+ V_2 n_{e2} n_{2+} S_{10} (\frac{3}{2} T_e + \frac{3}{2} T_{2+} + \Delta E_{10})$$
$$- V_o (\frac{3}{2} n_{10} T_{10} - T_w) \frac{(1 - R_E)}{\tau_w}$$

where T_w is the wall temperature, taken as 10^{-1} eV in this model and R_E is the reflection coefficient of neutrals hitting the wall.

$R_E = 0.93 - 0.02\ T_e$ is a rough approximation to results obtained from computer studies of wall reflection /4/. τ_w is the wall collision time given by the formula

$$\tau_w = \frac{r_o^2\ (n_{10} + n_{20})\sigma_e}{v_i}$$

where σ_e is the cross-section for neutral-neutral elastic collisions, ($\sigma_e \sim 5 \cdot 10^{-19}$ m^2) and v_i is the neutral thermal velocity.

H_2^o energy equation:

$$\frac{d}{dt}\left((V_1 - V_o + V_2)\frac{3}{2}\ n_{20}T_{20}\right) = -\frac{3}{2}T_{20}\left\{V_2 n_{e2} n_{20}(S_2+S_3+S_4+S_5) + V_2 n_{1+} n_{20} S_8\right\}$$

$$+ V_2 n_{2+} n_{20} S_9 \frac{3}{2}\ (T_{2+} - T_{20})$$

$$+ \frac{V_o}{2}\ \frac{n_{1+}}{\tau}\ \phi_1 \frac{3}{2} T_w + V_2 \frac{n_{2+}}{\tau}\ \phi_2 \frac{3}{2} T_w$$

$$- (V_1 - V_o + V_2)\ \frac{3}{2} n_{20}\ (T_{20} - T_w)\ \frac{(1-R_E)}{\tau_w}$$

Appendix B

Low-Z Impurity Effects

The effect of energy losses due to ionization and radiation of oxygen impurities was included in the model by considering the rate equations for each ionization state in the following manner /17,1/:

$$V_1 \frac{dO_1}{dt} = V_o \; -n_{eo} S_1 O_1 + n_{eo} \alpha_1 O_2 + \sum_{k=2}^{9} \frac{O_k}{\tau}$$

$$\frac{dO_k}{dt} = n_{eo} O_{k-1} S_{k-1} - n_{eo} O_k (S_k + \alpha_{k-1})$$

$$+ n_{eo} O_{k+1} \; _k - \frac{O_k}{\tau}$$

$$\text{for } k = 2,3 \ldots 8$$

$$\frac{dO_9}{dt} = n_{eo} O_8 S_8 - n_e O_9 \alpha_8 - \frac{O_9}{\tau}$$

where O_k is the density of the k^{th} ionization state so that O_1 is the neutral atom and O_9 the fully stripped oxygen ion, O^{+8}

S_k is the ionization rate of the k^{th} state /17/

α_k is the radiative recombination rate (three-body recombination rates are very small and therefore neglected).

The total power loss rate P_{imp} is given by the sum of ionization P_{ion}, and radiation losses P_{rad}.

where $P_{ion} = \sum_{j=1}^{8} \chi_j n_{eo} S_j O_j + \frac{3}{2} k T_e \alpha_j n_e O_{j+1}$

χ_j is the ionization energy of the j^{th} state.

For the radiation power loss, the formula developed by Düchs and Griem /18/ has been used.

$$P_{rad} = 2 \cdot 10^{-8} \chi_H \sqrt{\frac{\chi_H}{T_e}}\, n_{eo} \left(O_2\, e^{\frac{-16}{T_e}} + O_3 e^{\frac{-18}{T_e}} + 1.5\, O_4\, e^{\frac{-19}{T_e}}\right.$$

$$+ 1.25\, O_5 e^{\frac{-20}{T_e}} + O_6 \left(e^{\frac{-12}{T_e}} + 0.5\, e^{\frac{-83}{T_e}}\right)$$

$$\left. + 1.25\, O_7 e^{\frac{-575}{T_e}} + 0.75\, O_8 e^{\frac{-655}{T_e}}\right)$$

where χ_H is the ionization energy of hydrogen

(T_e is in eV and n_{eo} in cm^{-3})

The total electron density in the presence of impurities is given by

$$n_{eo} = n_{1+} + \frac{V_2}{V_o}\, n_{2+} + \sum_{k=2}^{9} z_k O_k$$

and $$Z_{eff} = \frac{n_{eo}}{n_{1+} + \frac{V_2}{V_o}\, n_{2+} + \sum_{k=2} O_k}$$

References

/1/ HAWRYLUK, R.J., SCHMIDT, J.A., Nucl. Fusion 16 (1976) 775; HAWRYLUK, R.J., Bull.Amer.Phys.Soc. 23 (1978) 832

/2/ PAPOULAR, R., Nucl. Fusion 16 (1976) 37.

/3/ McALEES, D.G., MARCUS, F.B., ATTENBERGER, S.E., CHERDACK, R.N., KERBEL, C.D., McNALLY, J.R.Jr., PENG, Y.-K., M., SCHILLING, G., STRICKLER, D.J., UCKMAN, N.A., Plasma Engineering in a Deuterium-Tritium Fueled Tokamak, ORNL/TM-5573, Oak Ridge (October 1976)

/4/ MARCUS, F.B., ATTENBERGER, S.E., private communication

/5/ WAIDMAN, G., Zur Zündphase einer Tokamakentladung, KFA-Jülich-1467, November 1977

/6/ HUTCHINSON, I.H., STRACHAN, J.D. Nucl. Fusion 14(1974) 649

/7/ ALLGEYER, R. at al.,Proc. 6th Symp. on Engin. Probl. of Fusion Research (1976) 378

/8/ HINNOV, E., BISHOP, A.S., FALLON Jr, H., Plasma Physics 10 (1968) 291

/9/ KNOEPFEL, H., SPONG, D.A. Review Paper: "Runaway Electrons in Toroidal Discharges" Nucl.Fusion 19 (1979) 785

/10/ TFR Group, Nucl.Fusion 16 (1976) 473

/11/ GUREVICH, A.V. Soviet Phys.-JETP 12 (1961) 904

/12/ KNOEPFEL, H., SPONG, D.A., ZWEBEN, S.J. Physics of Fluids 30 (1977) 511

/13/ Peng, Y.-K., M., BOROWSKI, S.K., KAMMASH, T. Nucl.Fusion 18 (1978) 1489

/14/ KÖPPENDÖRFER, W., Nucl. Fusion 19 (1979) 1319

/15/ TFTR - Final Conceptual Design Report, PPPL - 1275, Febr. 1976, Chapter 3

/16/ HINNOV, E., BISHOP, A.S., HOFMAN, F.W., "Interpretation of Atomic Hydrogen Light in the C Stellarator" Princeton Plasma Phys. Laboratory Report, MATT-270, May 1964

/17/ DÜCHS, D., Fluid Models for Tokamak Plasmas, NRL Report 7340, Washington (1972)

/18/ DÜCHS, D., GRIEM, H.R., Phys. of Fluids 9 (1966) 1099

Table I

Reaction	Rate Coefficient	E(eV)	ΔE(eV)
$e + H_1^o \rightarrow e + H_1^+ + e$	S_1	13.6	–
$e + H_2^o \rightarrow e + H_2^+ + e$	S_2	16.5	–
$e + H_2^o \rightarrow e + H_1^+ + H_1^o + e$	S_3	30.0	11.5
$e + H_2^o \rightarrow e + H_1^o + H_1^o$	S_4	11.0	6.5
$e + H_2^o \rightarrow e + H_1^+ + H_1^+ + e + e$	S_5	48.0	13.0
$e + H_2^+ \rightarrow e + H_1^+ + H_1^o$	S_6	6.0	3.5
$H_1^+ + H_1^o \rightarrow H_1^o + H_1^+$	S_7	-	-
$H_1^+ + H_2^o \rightarrow H_1^o + H_2^+$	S_8	-	-
$H_2^+ H_2^o \rightarrow H_2^o + H_2^o$	S_9	-	-
$e + H_2^+ \rightarrow H_1^o + H_1^o$	S_{10}	-	4.0
$e + H_1^o(n=1) \rightarrow e + H_1^o(n=2)$	S_{2x}	10.2	-
$e + H_1^o(n=2) \rightarrow e + H^o(n=3)$	S_{3x}	12.1	–
$e + H_1^o(n=3) \rightarrow e + H_1^o(n=4)$	S_{4x}	12.8	-

Figure Captions

Fig. 1: Geometry of the Plasma Model indicating the three different regions of the discharge considered.

Fig. 2: Equivalent Circuit used to describe the coupling between the plasma and the OH circuit.

Fig. 3: Example of start-up behaviour described by the Model.

3a: Temperatures (in keV) - electron temperature (full line)
H_1^+ temperature (dashed line)

Densities (in m^{-3}) - electron density (upper full line)
H_2^o density (dashed line)
H_2^o density (lower full line)

Voltages - total loop voltage (upper line)
resistive voltage (lower line)

Discharge conditions:
BT - toroidal magnetic field (Tesla)
R1 - vacuum chamber radius (meters)
RA - plasma limiter radius (meters)
RR - major radius of plasma (meters)
BZ - transverse magnetic field (Tesla)
RV - discharge resistance (Ohm)
TSW - time at which discharge resistance is switched to the second value given for RV

Initial densities in m^{-3}:
DIH1N - H_1^o DIH2N - H_2^o
DIP1 - H_1^+ DIP2 - H_2^+

Loss coefficients:
Total loss rate = DBO. Bohm loss + DCU.Curvature Loss + DPC. Pseudoclassical Loss + DVF. Transverse Field Loss
PS1 = Ψ_1, PS2 = Ψ_2, PH1 = ϕ_1, PH2 = ϕ_2
TEW = T_w REC = R_E wall reflection coefficient

Gas Puff Rate:
PNRAT in $m^{-3}s^{-1}$
Start puff at TGS and finish at TGF
EI - initial temperatures of ions and electrons in keV

OH circuit parameters:
RE1 - OH circuit resistance (Ohm)
CL - self inductance of OH circuit (Henry)
CM - mutual inductance between plasma and OH circuit (Henry)
DN - internal density normalization factor

3b: Plasma Radii - plasma radius, r_1 (full line)
neutral penetration radius r_2 (dashed line)

REX coefficient of expansion of plasma radius, γ

$$\frac{A}{A_m} = \left(\frac{I}{I_m}\right)^{\gamma} \qquad A = \pi r_1^2$$

Fig. 4: Dependence of breakdown time, τ_B and flux required for breakdown, ϕ on applied loop voltage for two different values of the transverse field B_v. (τ_B is defined as the time required for 95 % of the neutrals to be ionized.)

H_2^o (o) = $1.0\ 10^{19}$ m^{-3} B = 3.0 T

r_1 = 0.3 m, r_o = 0.5 m R = 1.65 m

Preionization Fraction = 10^{-3}

Fig. 5: Variation of breakdown time, τ_B with transverse magnetic field, B_v for the same conditions as Figure 4.

Fig. 6: Results of Start-up calculations for varying neutral filling densities.

B_v = 0, preionization fraction is constant = 10^{-3}

Fig. 7: Variation of time required for breakdown, τ_B with pre-ionization density for different transverse magnetic field values.

R_v = 0.2 , r_1 = 0.4 m, r_2 = 0.5 m, B_r = 3 T

Total number of particles remains the same as used for the example in Figure 3 while the degree of preionization is varied.

Fig. 8: Illustration of the paths of plasma particles moving along magnetic field lines in the presence of a divertor field.

Fig. 9: Relation between area of closed field lines, A and the total plasma current, I for various multipole configurations including that of ASDEX

$$\frac{A}{A_m} = \left(\frac{I}{I_m}\right)^{\gamma}, \quad \gamma = 0.372 \text{ for ASDEX}$$

Fig. 10 a,b: Results of Start-up calculations with an expanding Magnetic Limiter produced by the Divertor Field configuration for the same conditions as given in Figure 3. (EDSF is the scale factor for the electron density variation.)

Fig. 11
a,b: Magnetic Limiter Start-up Behaviour for conditions as in Figure 10 except that γ = 0.2 corresponding to a reduced divertor field during start-up.

Fig. 12
a,b: Start-up Behaviour with a Magnetic Limiter for the same conditions as Figure 10 except R_V=0.3 Ω corresponding to an increased loop voltage.

Fig. 13
a,b: Start-up with decreased initial filling density following by gas puffing such that the total quantity of neutral gas used is the same as in the results of Figure 3.

Fig. 14
a,b: Illustration of the effect of 1 % oxygen impurity content on the start-up behaviour for conditions the same as in Figure 3. The decay of the neutral oxygen density followed by the appearance of successively higher ionization states of the impurities corresponding to increased electron temperatures may be observed in the impurity evolution.

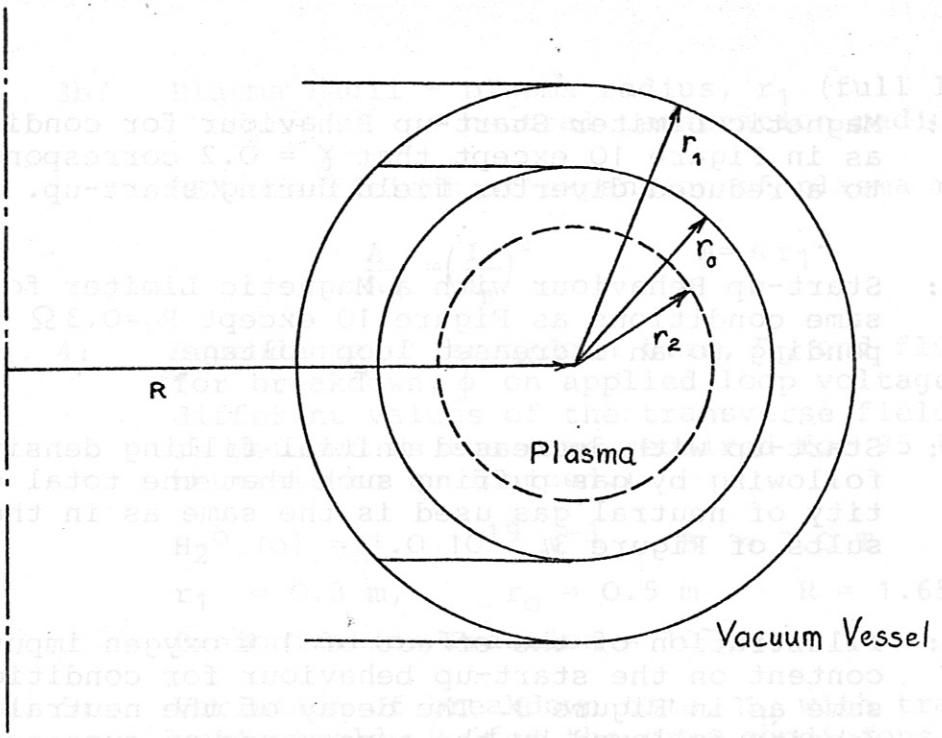

Figure 1

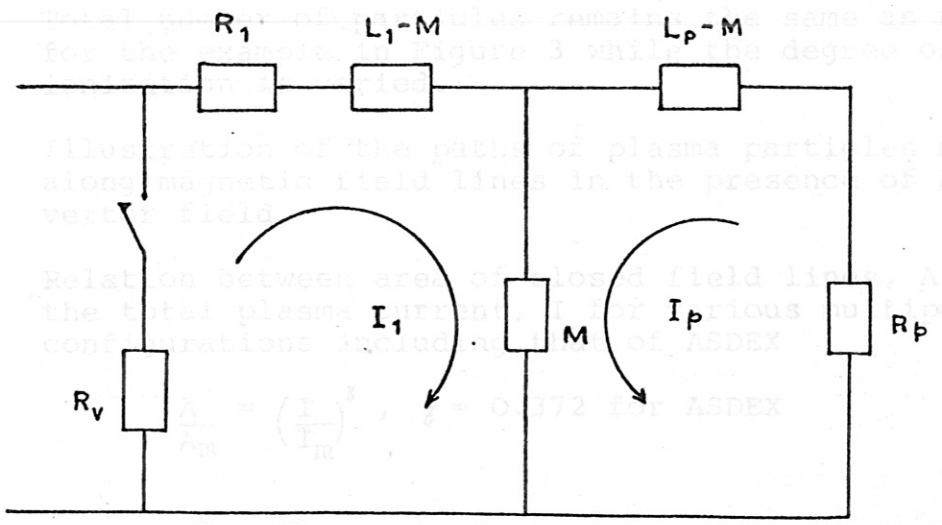

Figure 2

JBA117 23.OKT.79 12:54 K1-07 01 +

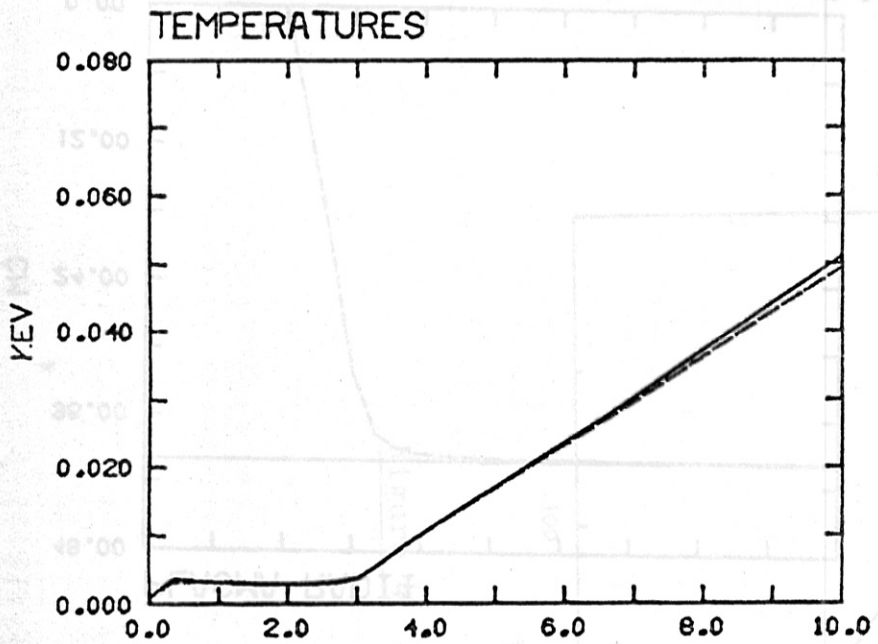

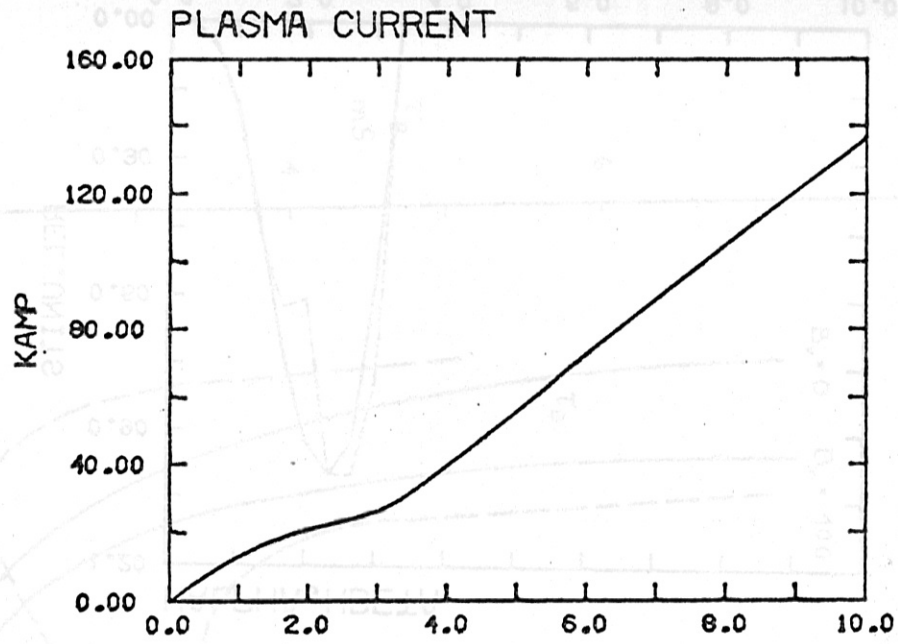

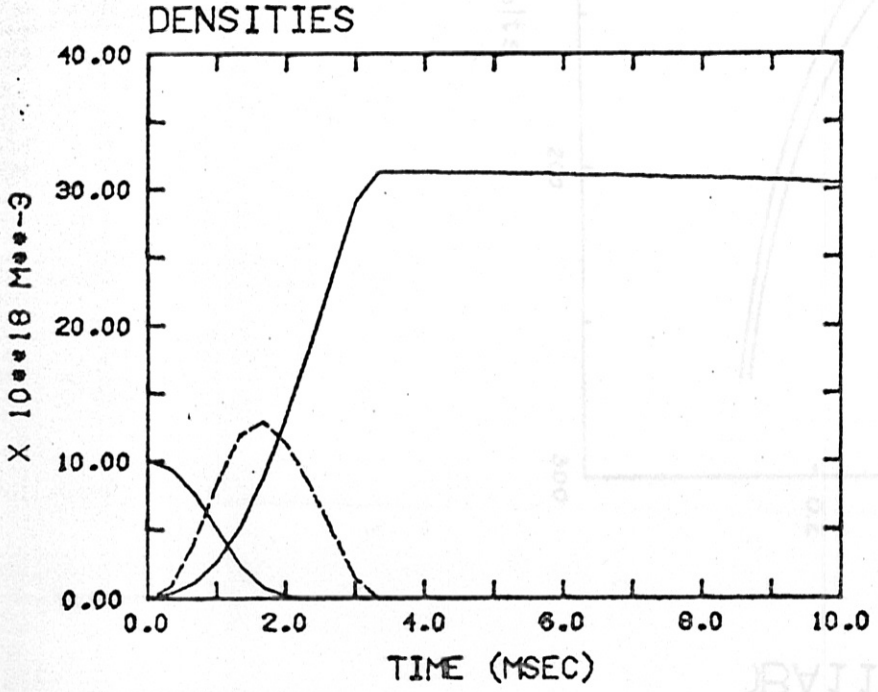

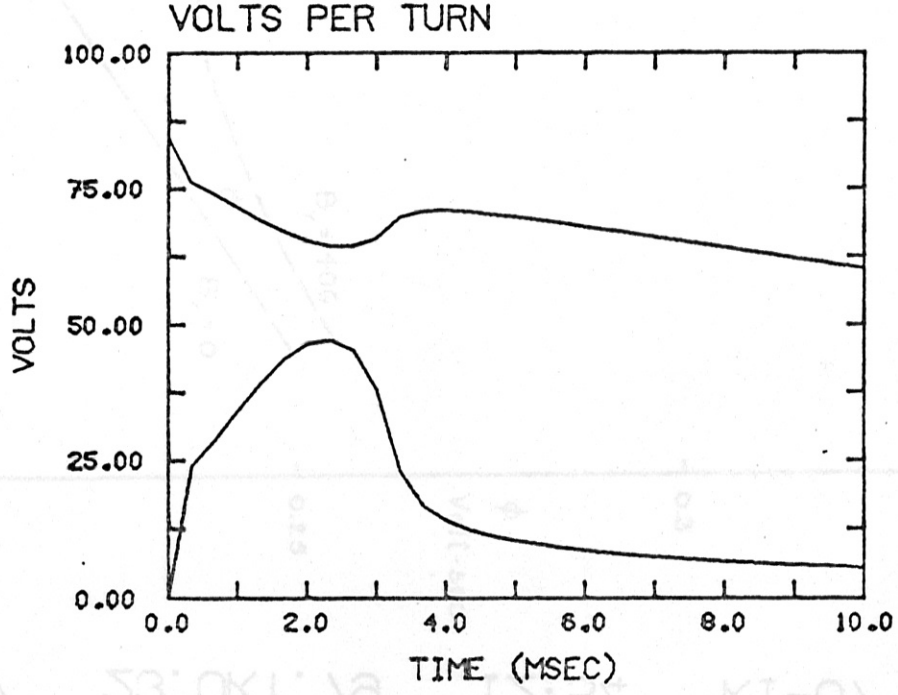

INPUT VALUES

BT	3.00
R1	0.50
RA	0.40
RR	1.64
BZ	0.0
RV	0.20 0.10
TSW	1.00E-02
DIH1N	0.10E 17
DIH2N	0.10E 20
DIP1	0.10E 17
DIP2	0.10E 17
DBO	1.00
DCU	0.00
DPC	0.00
DVF	0.00
PS1	0.00
PS2	0.00
PH1	0.00
PH2	0.00
TEW	1.00E-04
REC	1.00
NTOT	30
GAS PUFF	
PNRAT	0.10E 23
TGS	0.0
TGF	0.0
TEI	1.00E-03
RE1	0.15E-01
CL	0.84E-02
CM	0.84E-04
DN	0.10E 15

ASDEX

Figure 3a

)BA117 23.OKT.79 12:54 K1-07 02 +

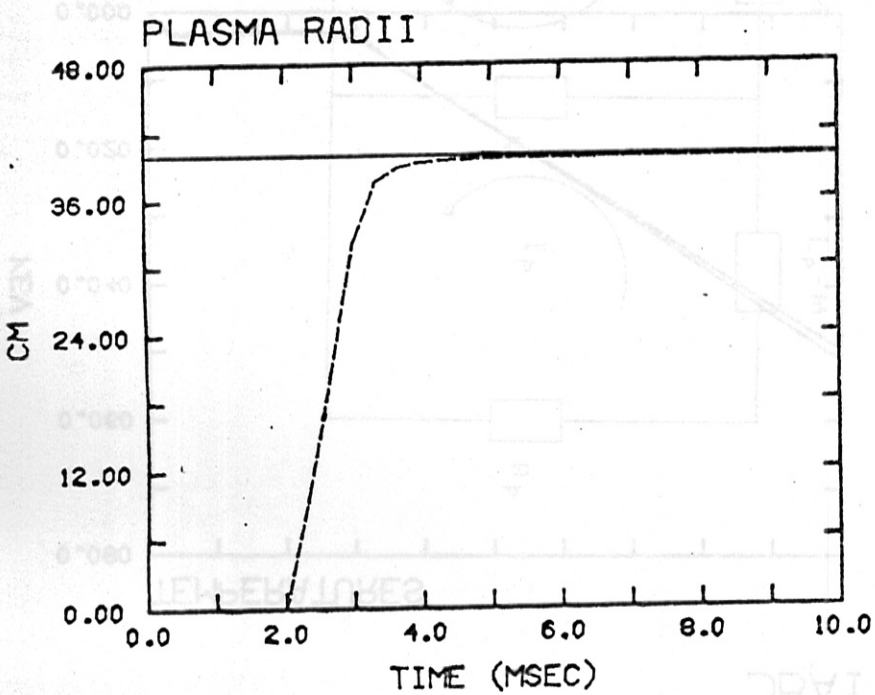

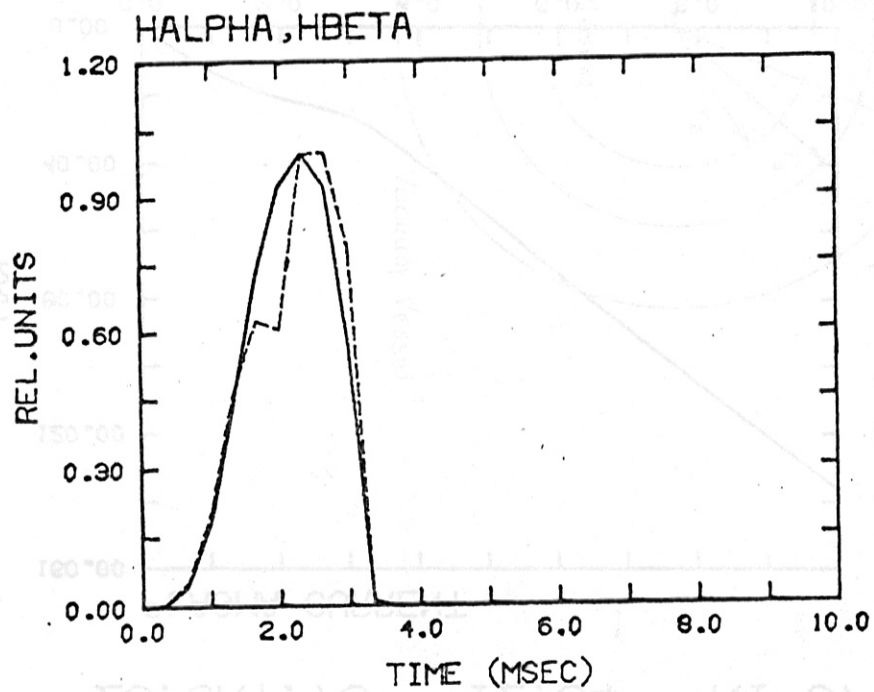

INITIAL RADIUS
R0 0.400

REX 0.0000

ASDEX

Figure 3b

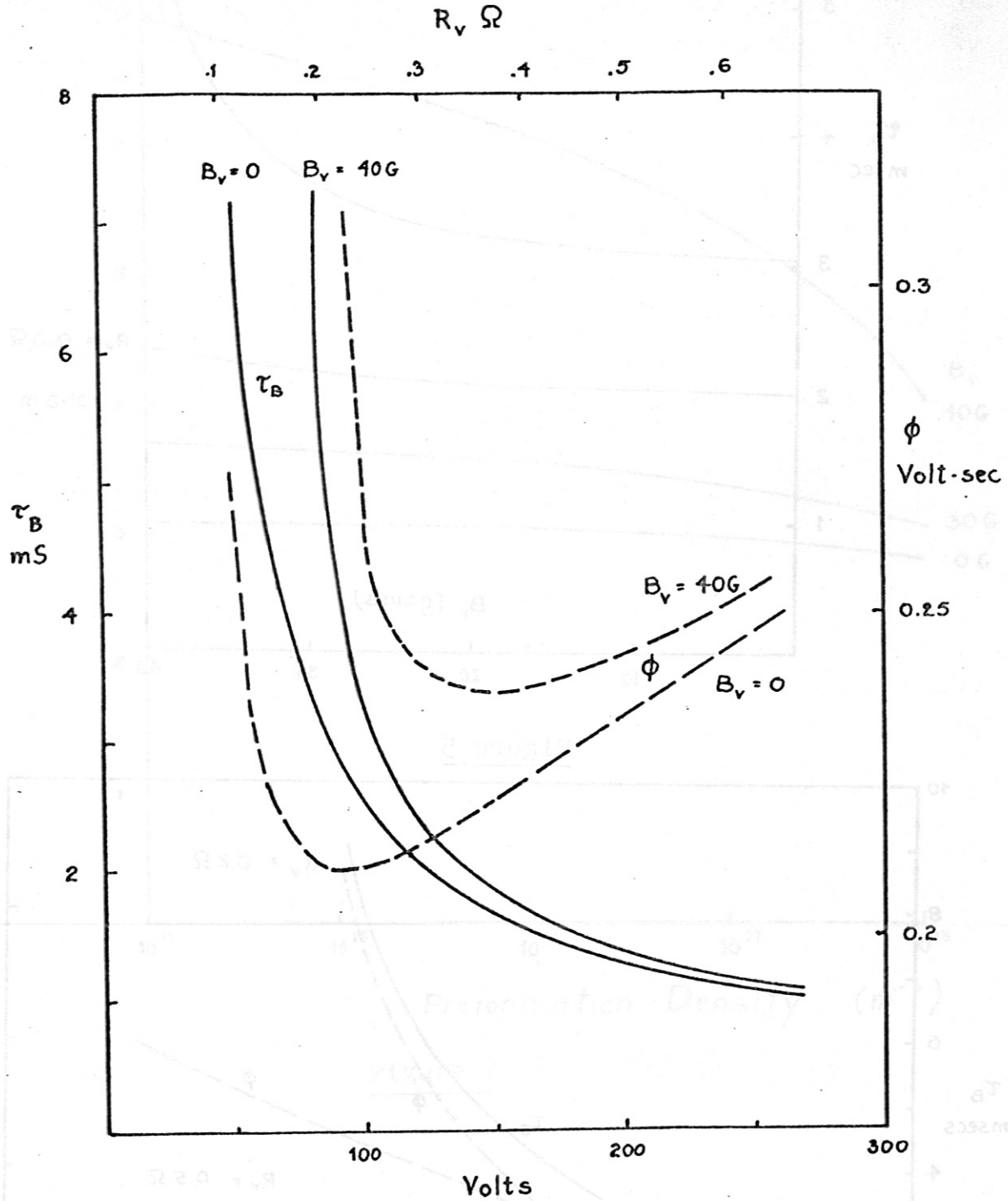
R_v Ω
.1
.2
.3
.4
.5
.6
8
6
4
2
B_v = 0
B_v = 40G
τ_B
τ_B mS
B_v = 40G
ϕ
B_v = 0
0.3
0.25
0.2
ϕ Volt-sec
100
200
300
Volts

Figure 4

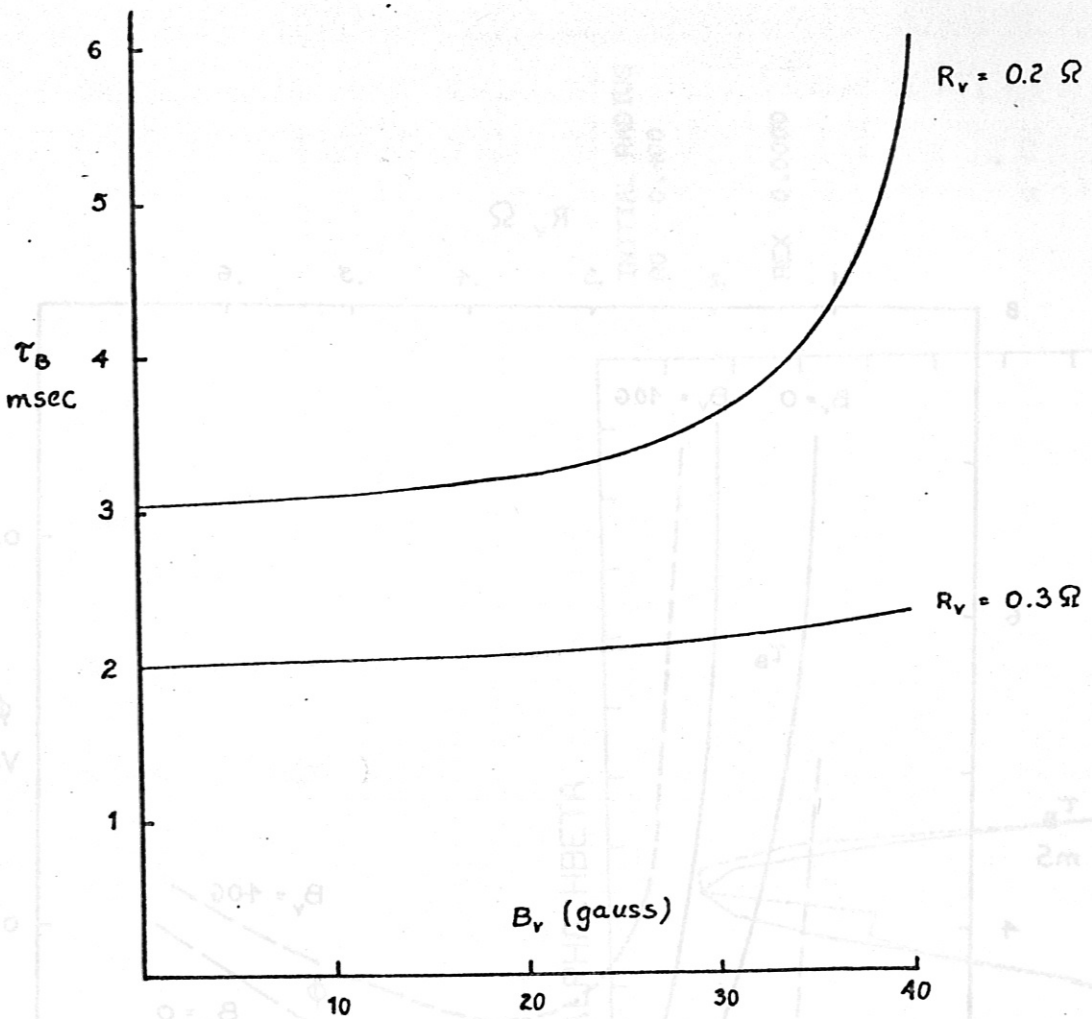

Figure 5

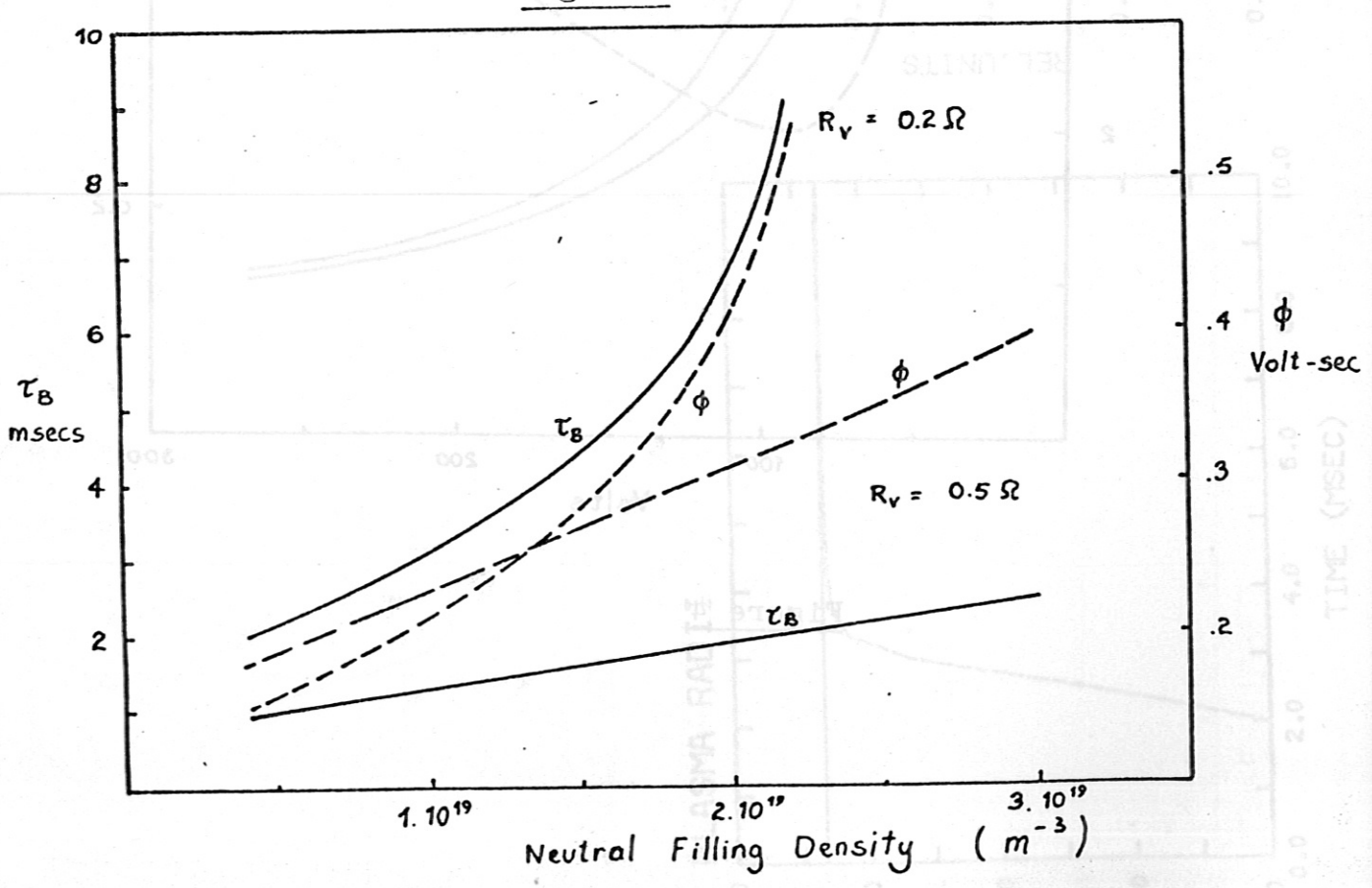

Figure 6

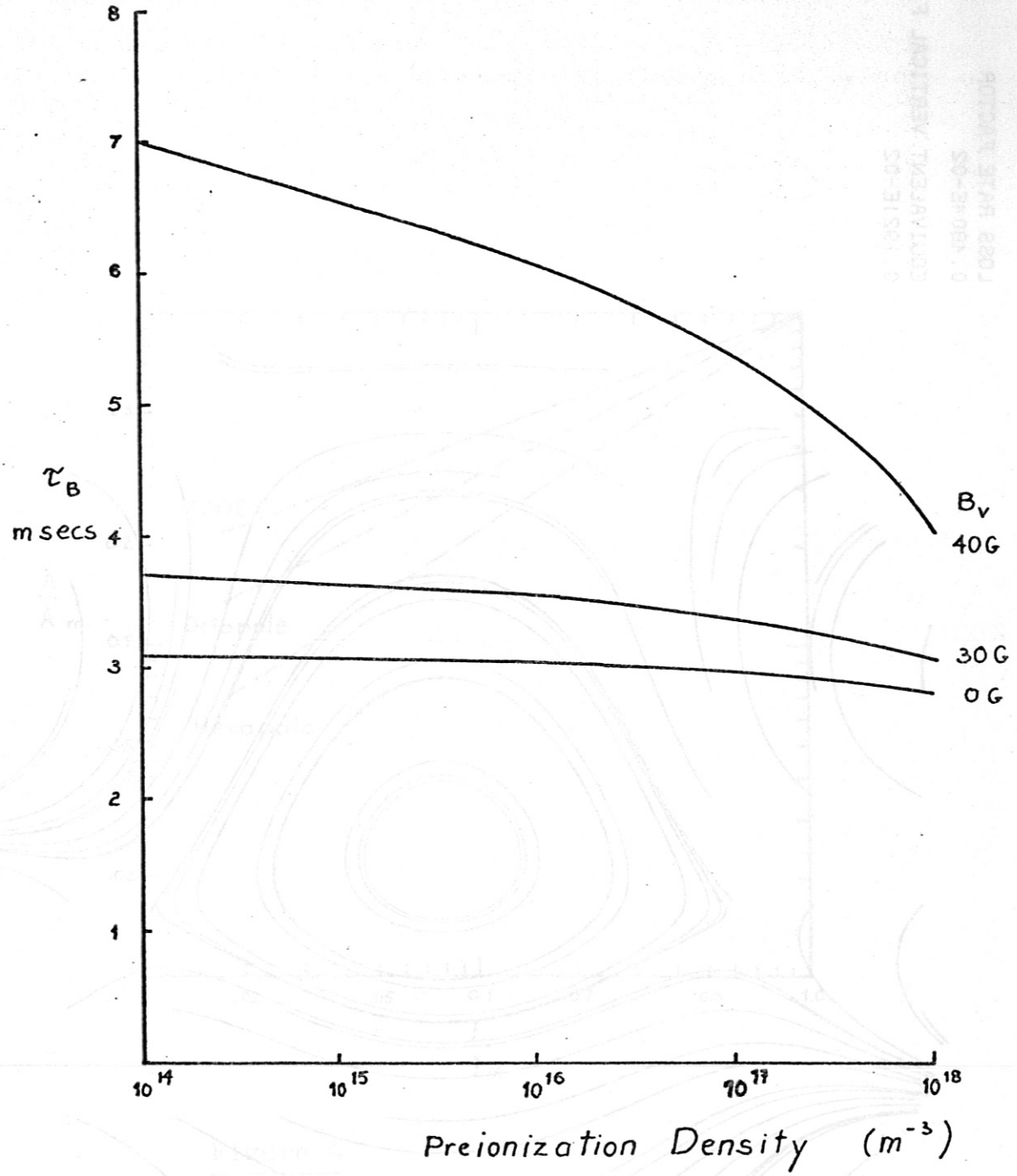
8
7
6
5
τ_B
msecs
4
3
2
1
B_v
40G
30G
0G
10^{14}
10^{15}
10^{16}
10^{17}
10^{18}
Preionization Density (m^{-3})

Figure 7

DBA695 22. JUN. 79- 14:55 K1-07 01 +

PARABOLIC CURRENT AND DENSITY DISTRIBUTION S

DIVERTOR CURRENT
50.00

PLASMA CURRENT (KA)
1.00

LOSS RATE FACTOR
0.4804E-02

EQUIVALENT VERTICAL FIELD
0.1921E-02

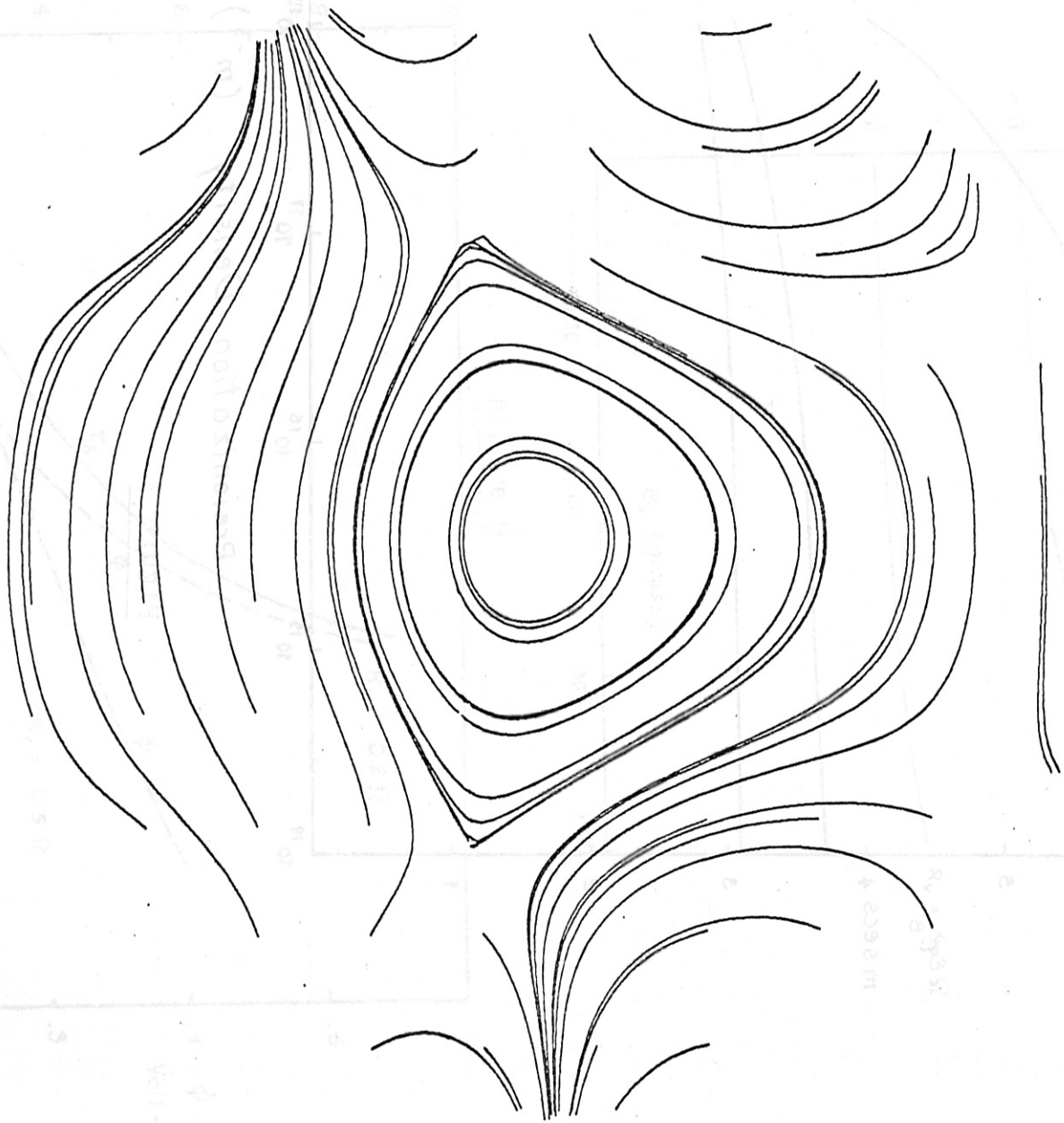

Figure 8

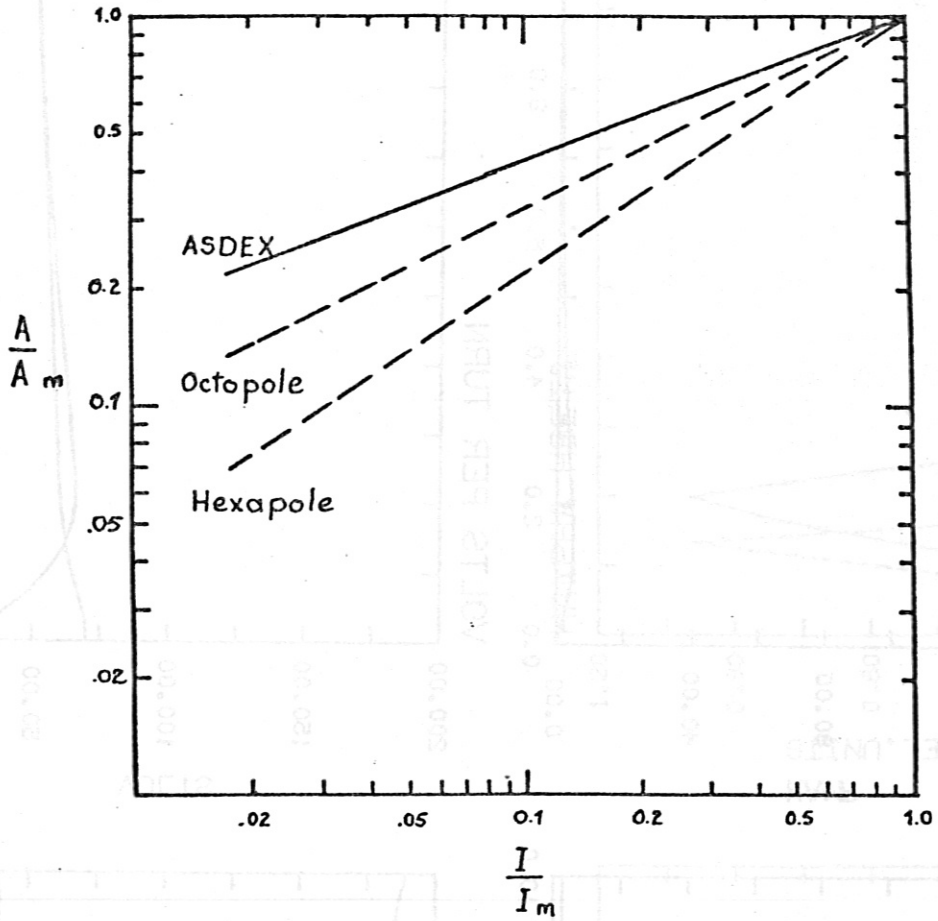
1.0
0.5
0.2
0.1
.05
.02
ASDEX
Octopole
Hexapole
A / A m
.02
.05
0.1
0.2
0.5
1.0
I / I m

Figure 9

DBA803 27.JUN.79 11:23 K1-07 01 +

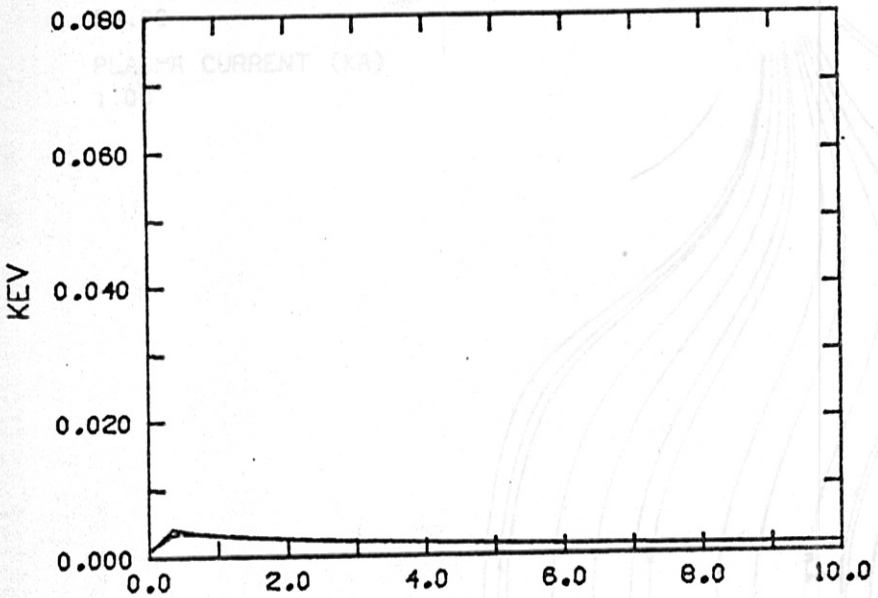

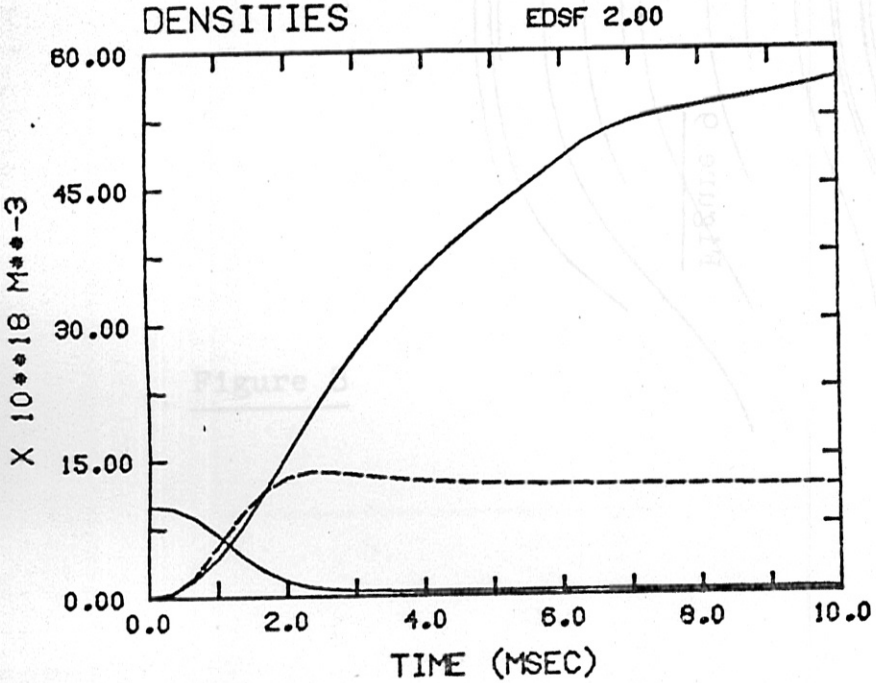

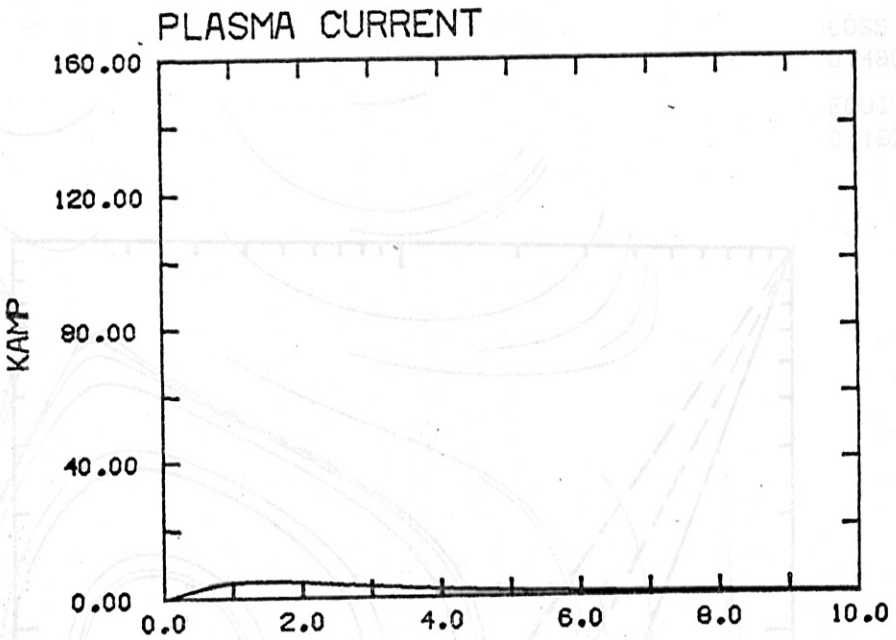

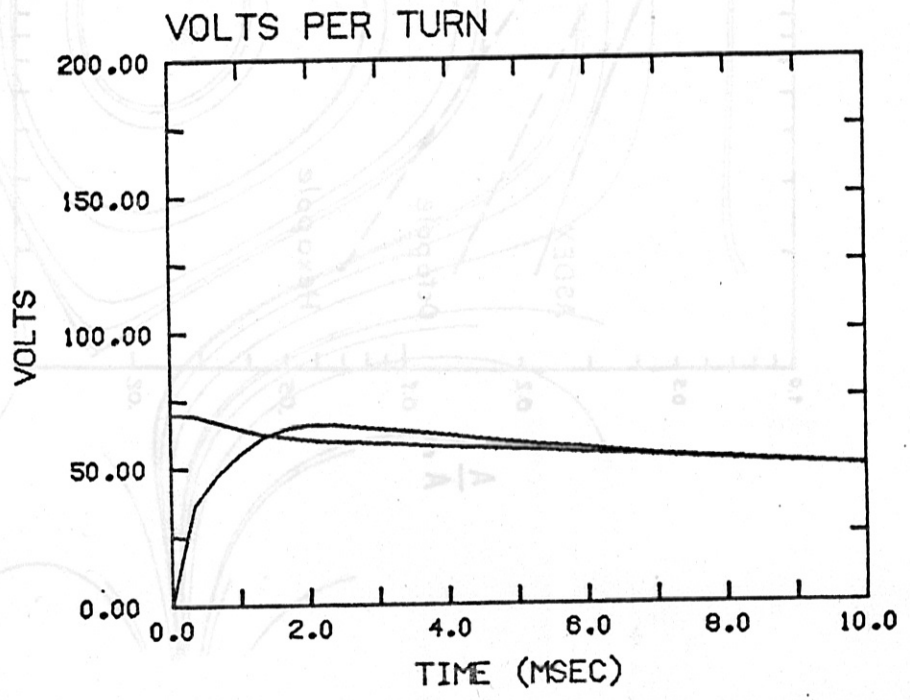

INPUT VALUES

BT	3.00
R1	0.50
RA	0.40
RR	1.64
BZ	1.00E-03
RV	0.20 0.10
TSW	1.00E-02
DIH1N0	.10E 17
DIH2N0	.10E 20
DIP1	0.10E 17
DIP2	0.10E 17
DBO	1.00
DCU	0.00
DPC	0.00
DVF	0.00
PS1	0.00
PS2	0.00
PH1	0.00
PH2	0.00
TEW	1.00E-04
REC	1.00
NTOT	30

GAS PUFF

PNRAT	0.10E 29
TGS	0.30E-02
TGF	0.0
TEI	1.00E-03
RE1	0.15E-01
CL	0.84E-02
CM	0.84E-04
DN	0.10E 15

Figure 10a

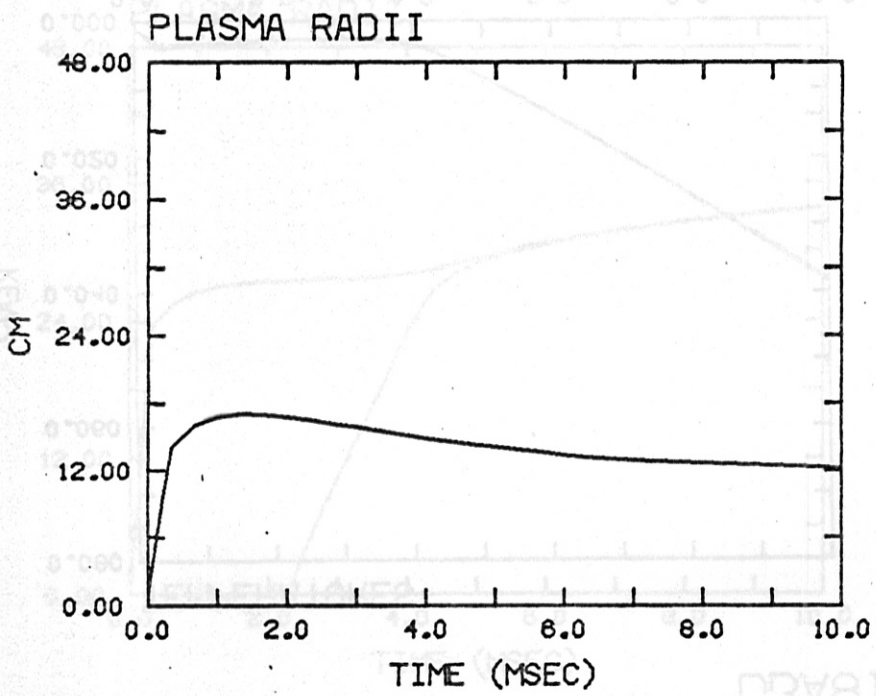

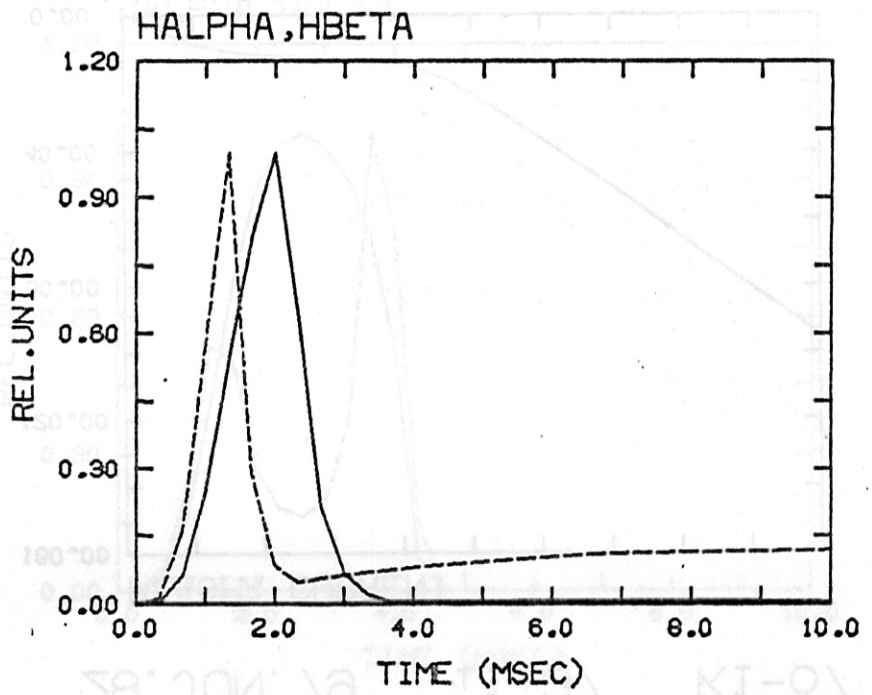

INITIAL RADIUS
R0 0.010

REX 0.3720

Figure 10b

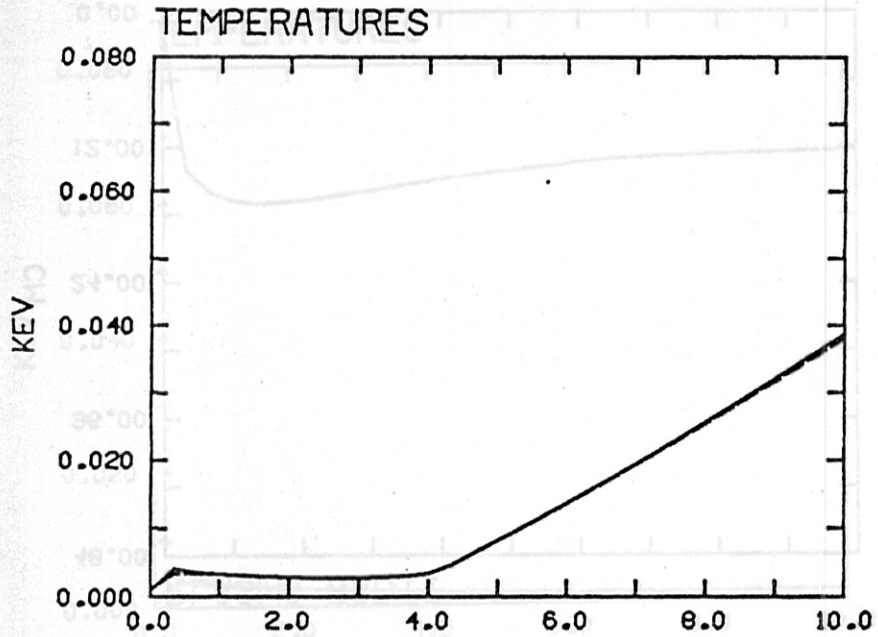

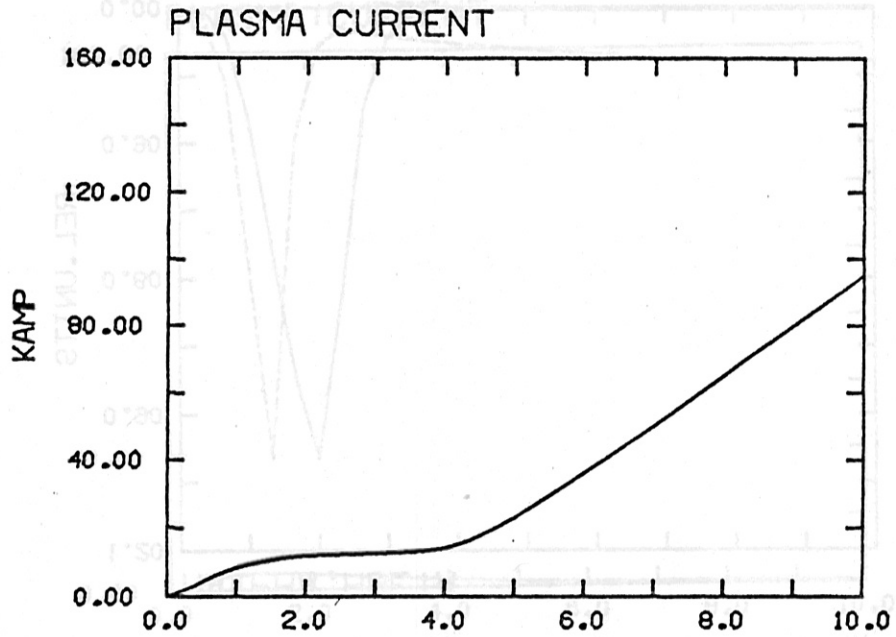

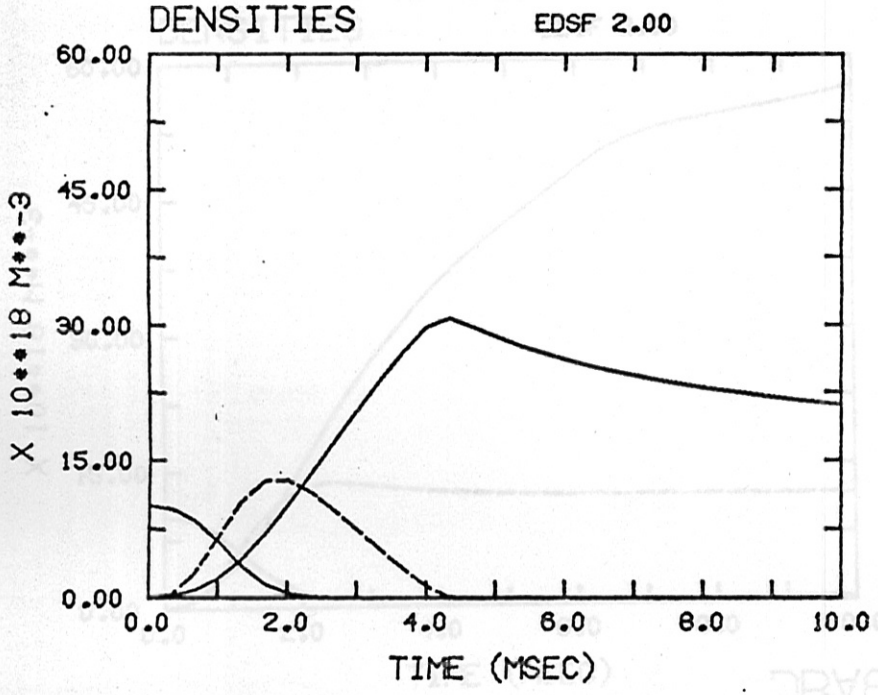

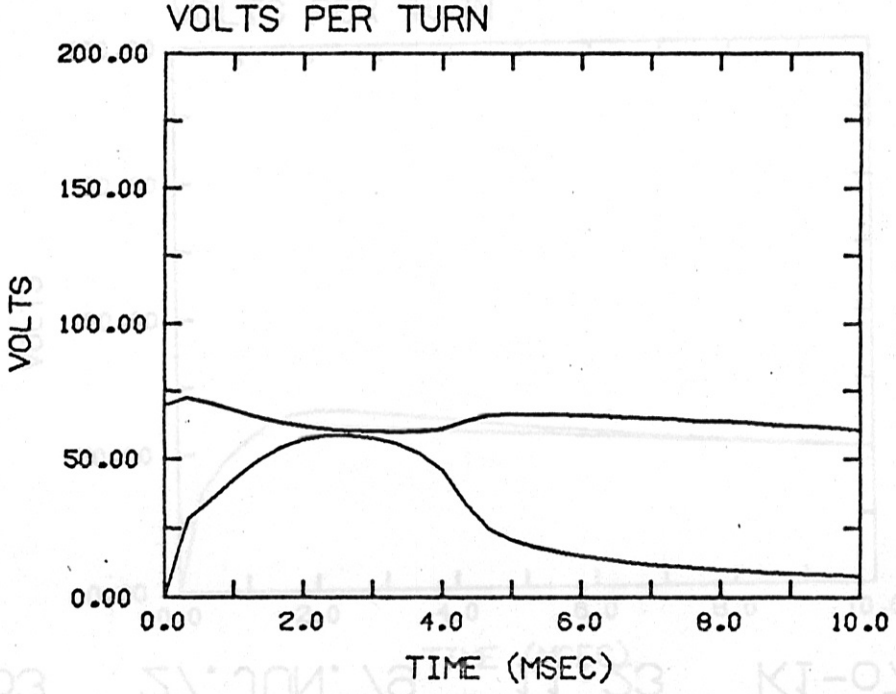

INPUT VALUES

BT	3.00
R1	0.50
RA	0.40
RR	1.64
BZ	1.00E-03
RV	0.20 0.10
TSW	1.00E-02
DIH1N	0.10E 17
DIH2N	0.10E 20
DIP1	0.10E 17
DIP2	0.10E 17
DBO	1.00
DCU	0.00
DPC	0.00
DVF	0.00
PS1	0.00
PS2	0.00
PH1	0.00
PH2	0.00
TEW	1.00E-04
REC	1.00
NTOT	30
GAS PUFF	
PNRAT	0.10E 23
TGS	0.30E-02
TGF	0.0
TEI	1.00E-03
RE1	0.15E-01
CL	0.84E-02
CM	0.84E-04
DN	0.10E 15

Figure 11a

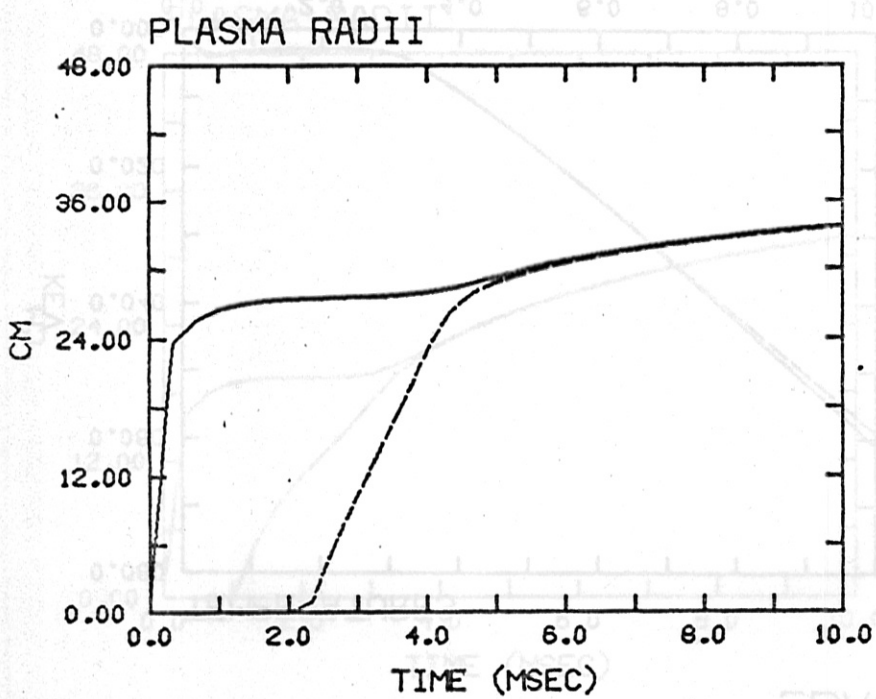

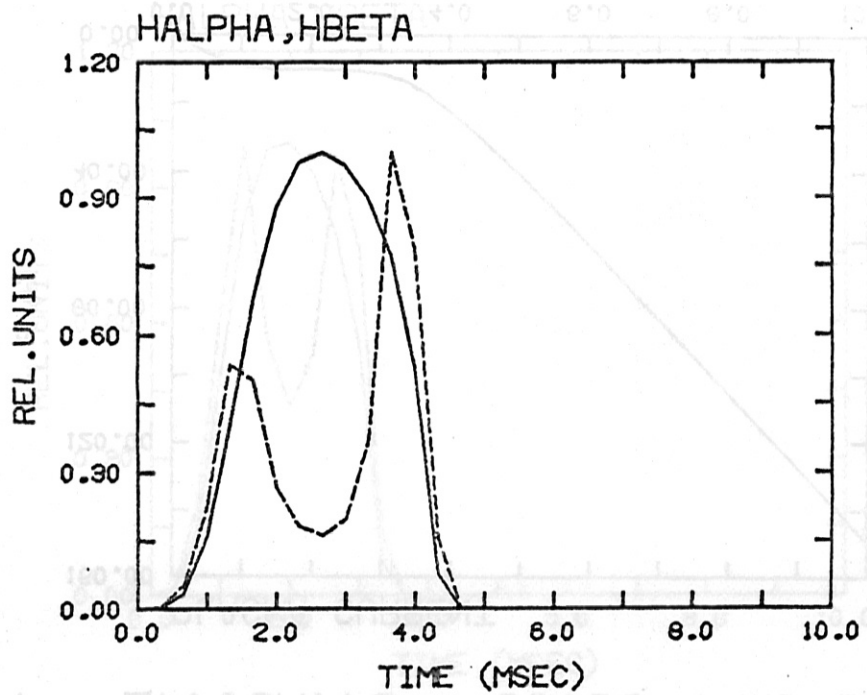

INITIAL RADIUS
R0 0.010

REX 0.2000

Figure 11b

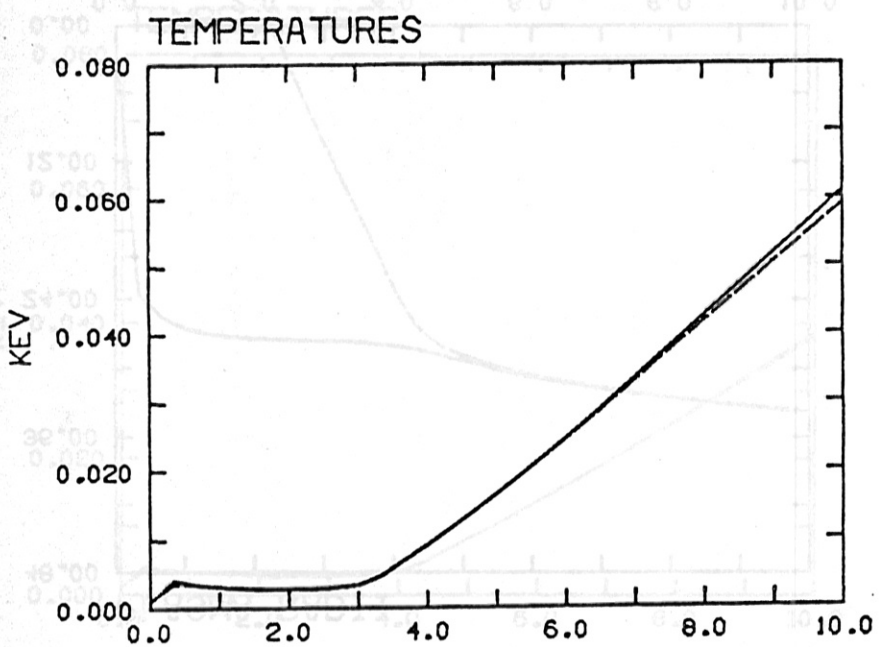

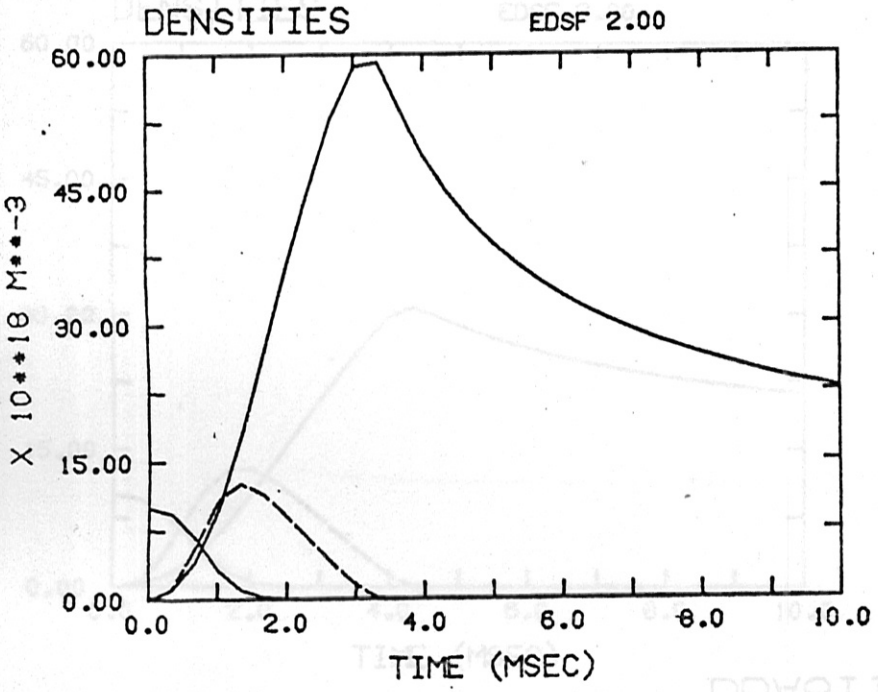

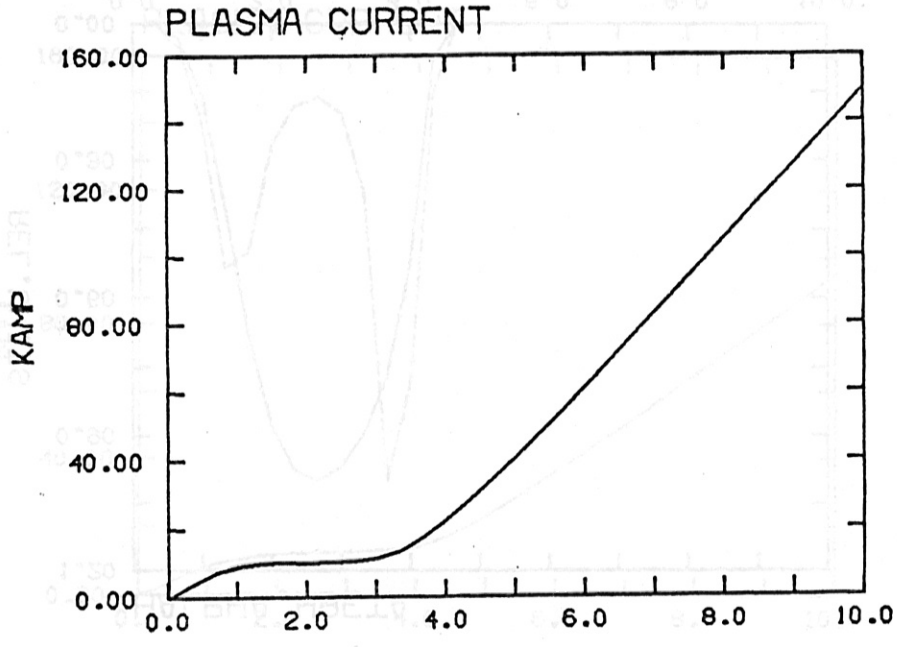

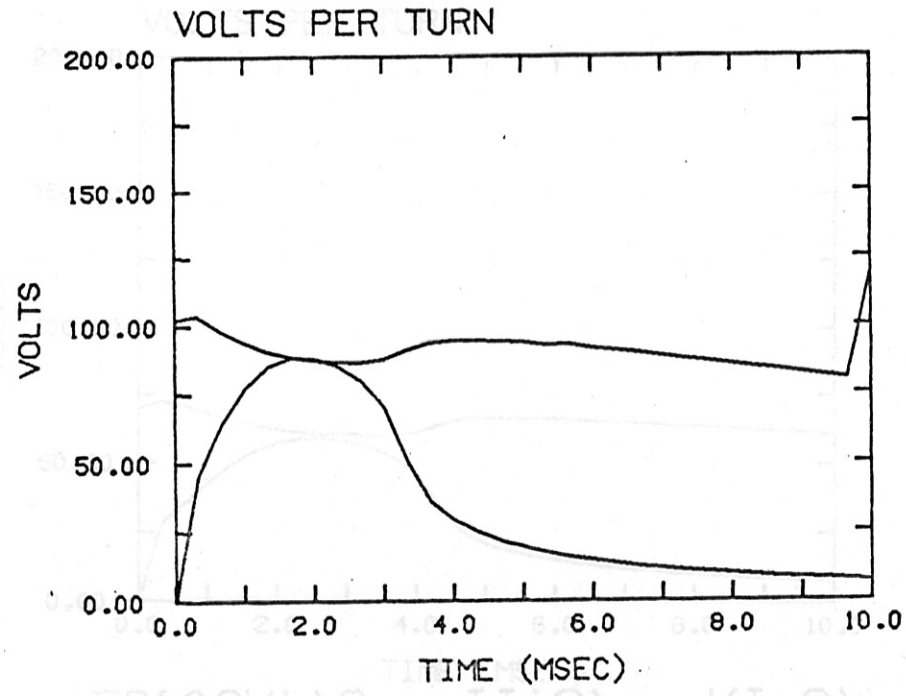

INPUT VALUES

BT	3.00
R1	0.50
RA	0.40
RR	1.64
BZ	1.00E-03
RV	0.30 0.10
TSW	1.00E-02
DIH1N	0.10E 17
DIH2N	0.10E 20
DIP1	0.10E 17
DIP2	0.10E 17
DBO	1.00
DCU	0.00
DPC	0.00
DVF	0.00
PS1	0.00
PS2	0.00
PH1	0.00
PH2	0.00
TEW	1.00E-04
REC	1.00
NTOT	30
GAS PUFF	
PNRAT	0.10E 23
TGS	0.30E-02
TGF	0.0
TEI	1.00E-03
RE1	0.15E-01
CL	0.84E-02
CM	0.84E-04
DN	0.10E 15

Figure 12a

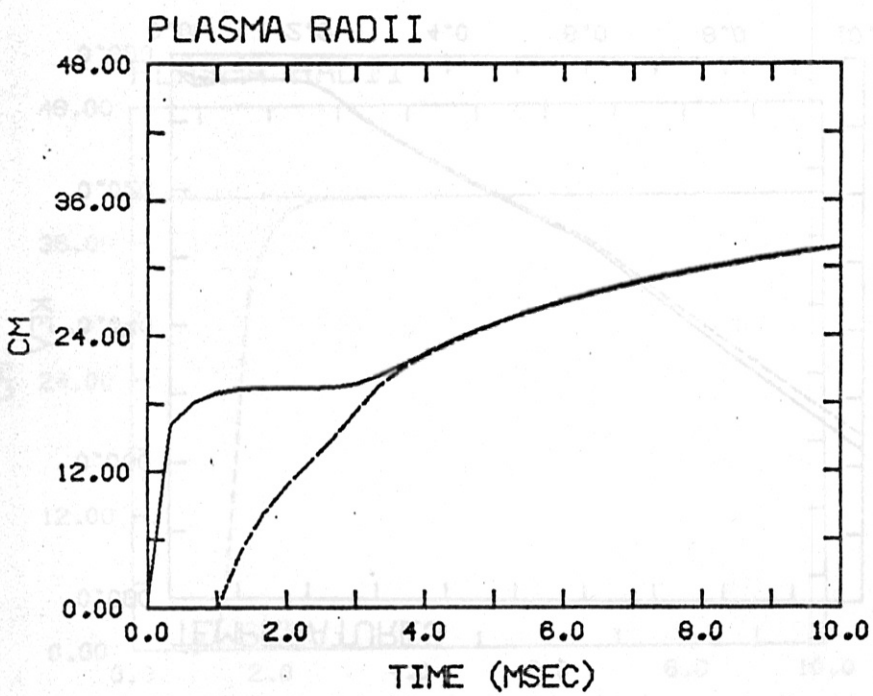

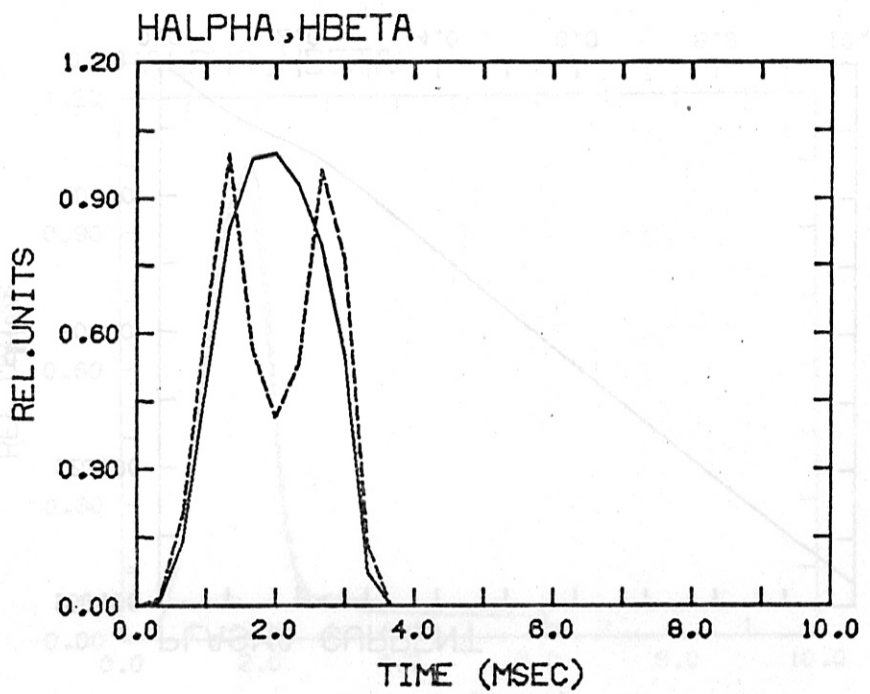

INITIAL RADIUS
R0 0.010

REX 0.3720

Figure 12b

DBA690 19.DEZ.79 07:33 K1-07 01 +

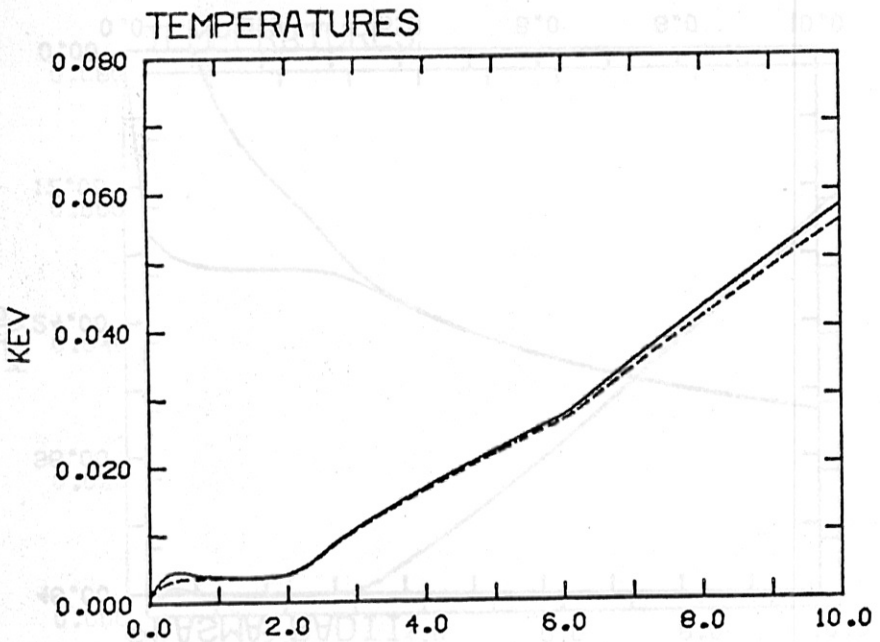

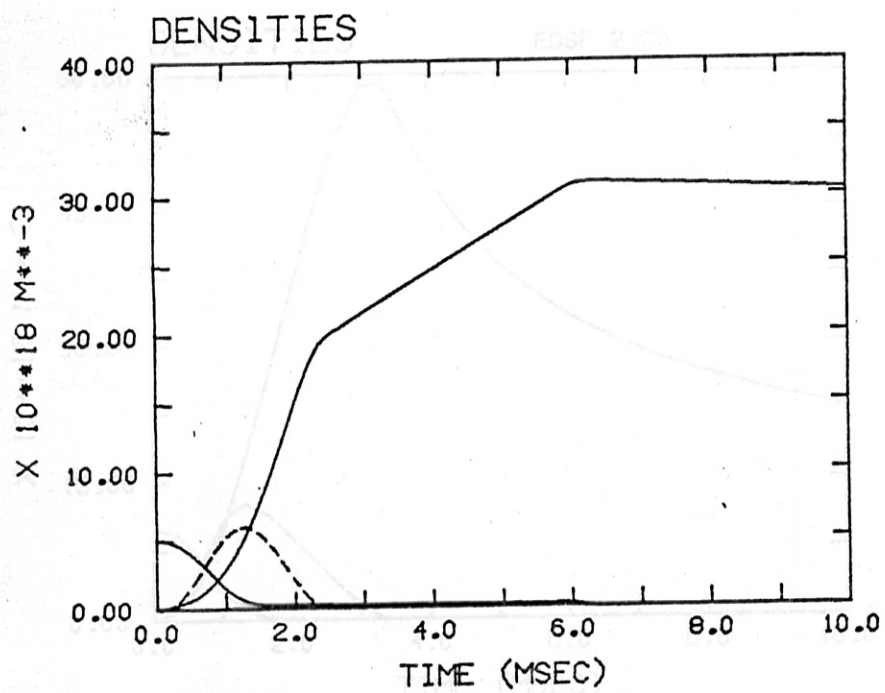

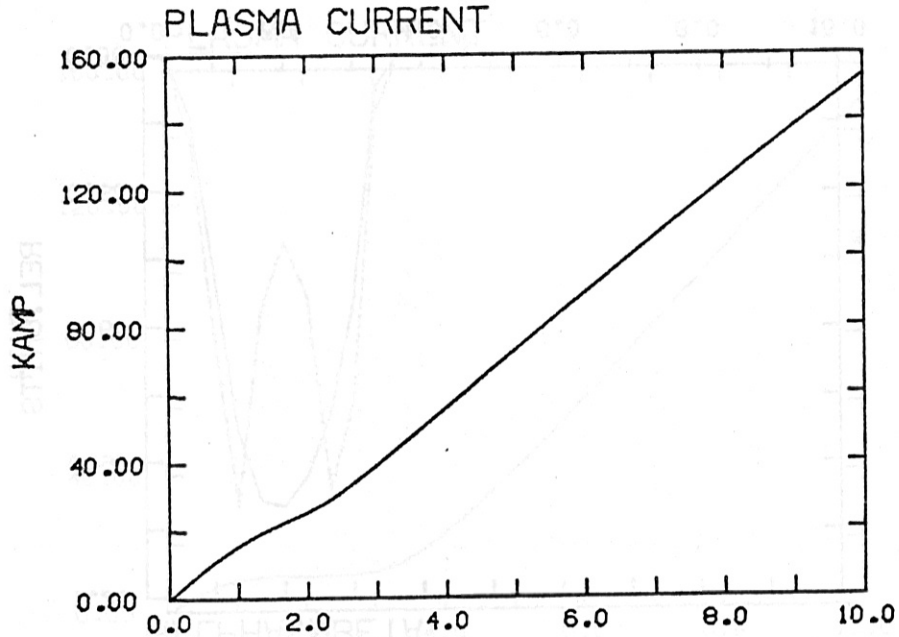

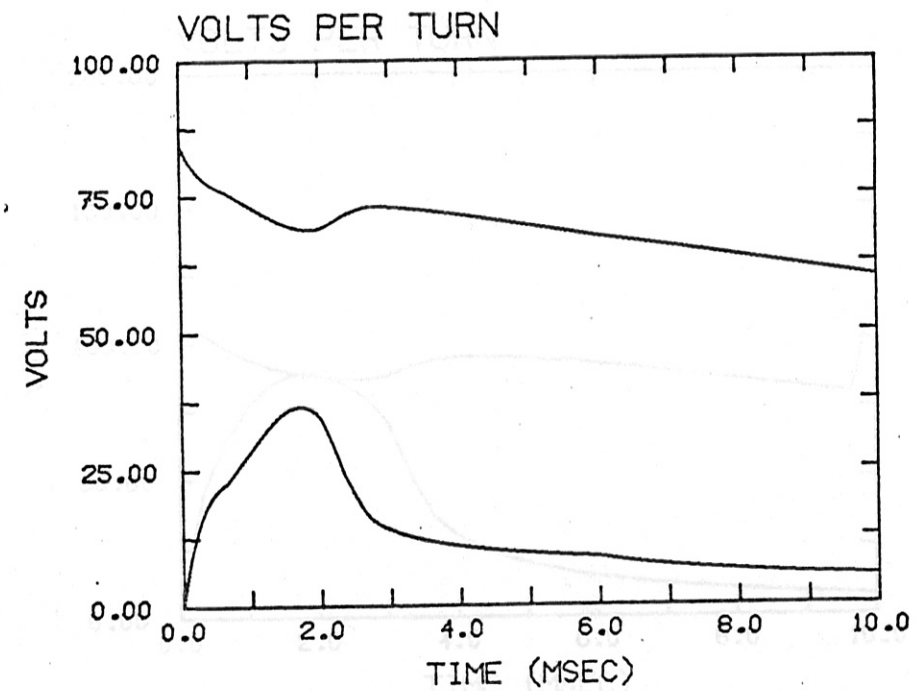

INPUT VALUES

BT	3.00
R1	0.50
RA	0.40
RR	1.64
BZ	0.0
RV	0.20 0.10
TSW	1.00E-02
DIH1N0	.10E 17
DIH2N0	.50E 19
DIP1	0.10E 17
DIP2	0.10E 17
DBO	1.00
DCU	0.00
DPC	0.00
DVF	0.00
PS1	0.00
PS2	0.00
PH1	0.00
PH2	0.00
TEW	1.00E-04
REC	1.00
NTOT	30
GAS PUFF	
PNRAT	0.81E 22
TGS	1.00E-03
TGF	0.60E-02
TEI	1.00E-03
RE1	0.15E-01
CL	0.84E-02
CM	0.84E-04
DN	0.10E 15

ASDEX

Figure 13a

DBA690 19.DEZ.79 07:33 K1-07 02 +

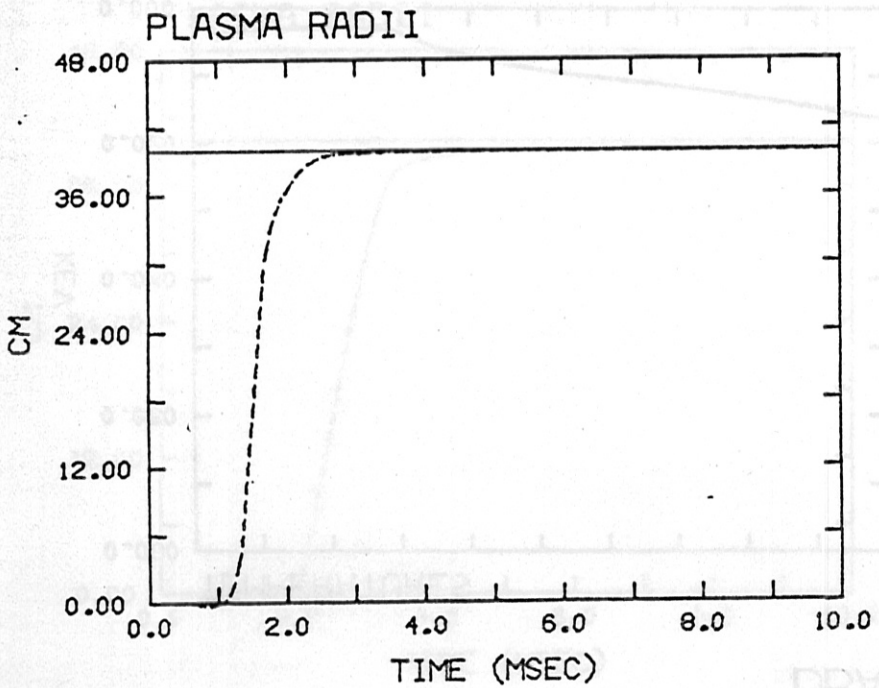

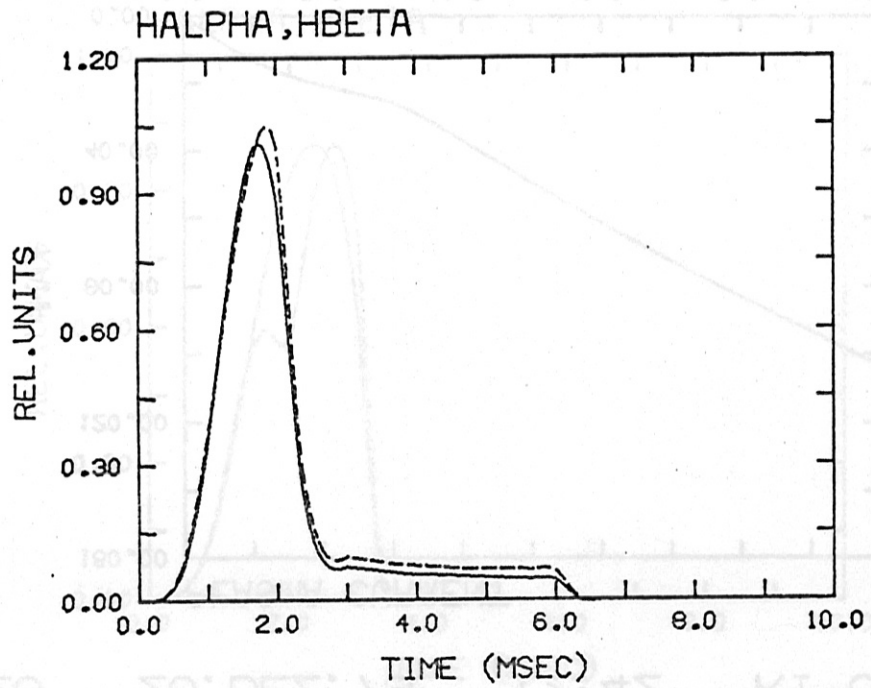

INITIAL RADIUS
R0 0.400

REX 0.0000

ASDEX

Figure 13b

DBA728 20. DEZ. 79 12:42 K1-07 01 +

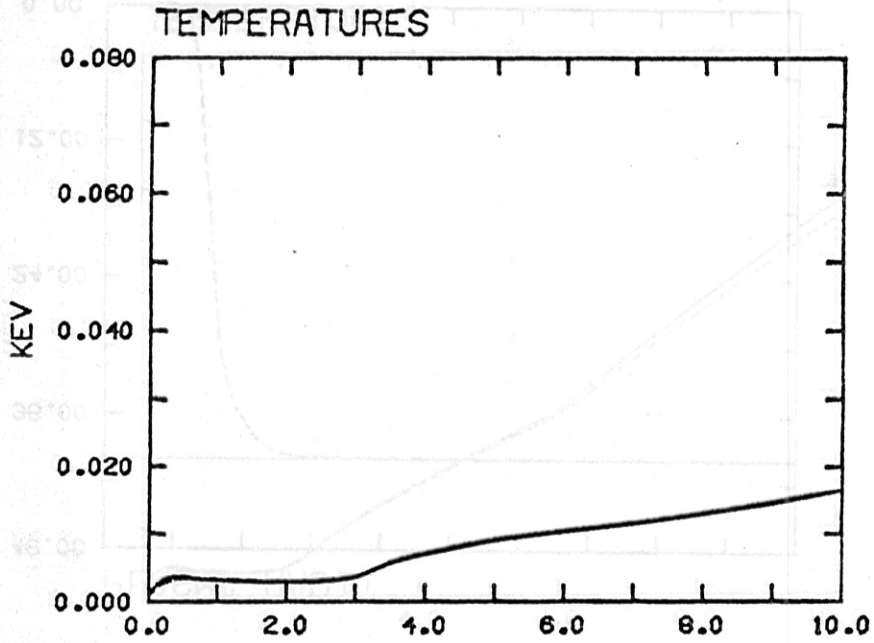

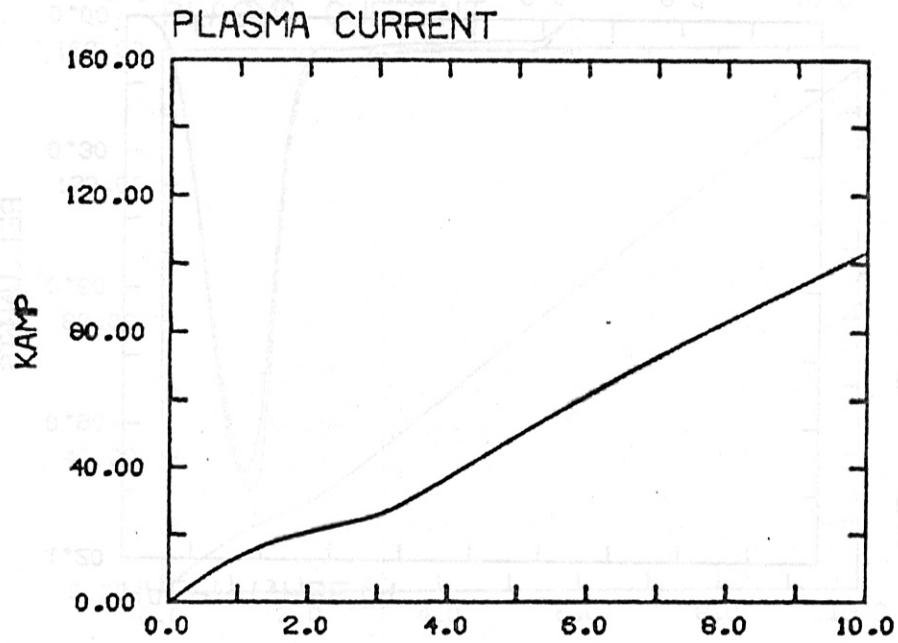

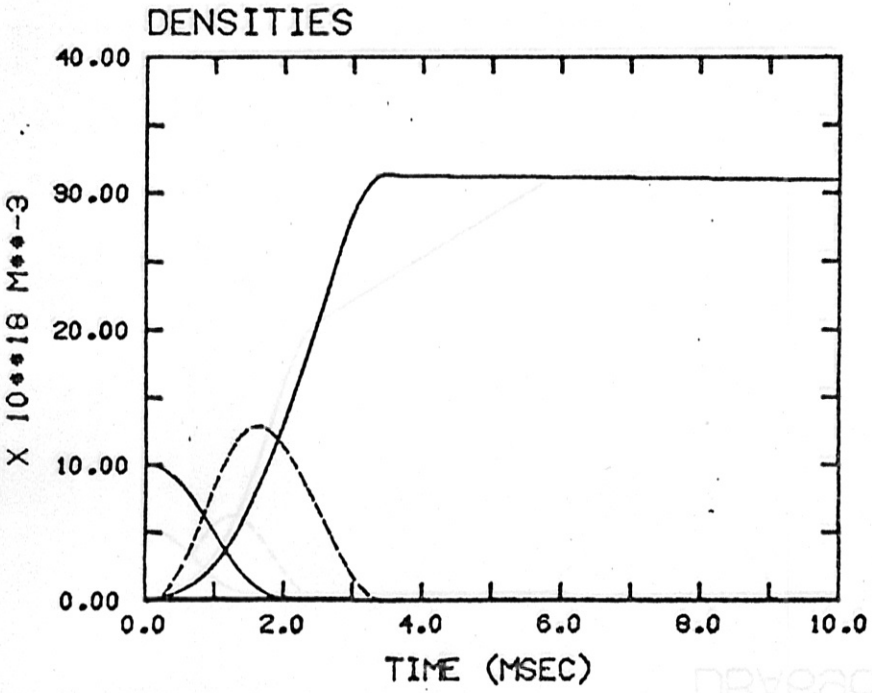

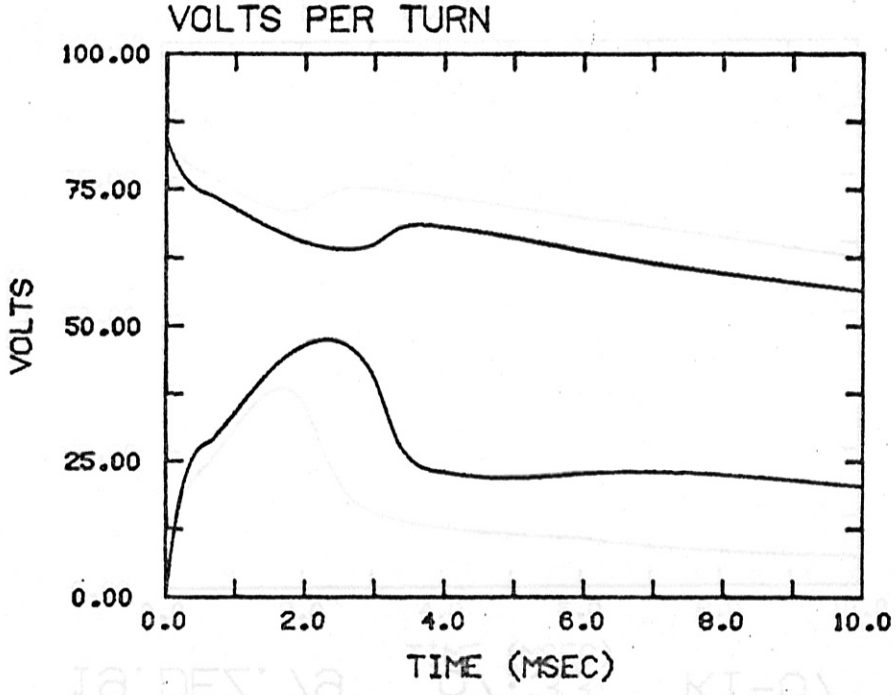

INPUT VALUES

BT	3.00
R1	0.50
RA	0.40
RR	1.64
BZ	0.0
RV	0.20 0.10
TSW	1.00E-02
DIH1N	0.10E 17
DIH2N	0.10E 20
DIP1	0.10E 17
DIP2	0.10E 17
DBO	1.00
DCU	0.00
DPC	0.00
DVF	0.00
PS1	0.00
PS2	0.00
PH1	0.00
PH2	0.00
TEW	1.00E-04
REC	1.00
NTOT	30
GAS PUFF	
PNRAT	0.20E 23
TGS	0.0
TGF	0.0
TEI	1.00E-03
RE1	0.15E-01
CL	0.84E-02
CM	0.84E-04
DN	0.10E 15

ASDEX

Figure 14a

DBA728 20. DEZ. 79 12:42 K1-07 02 +

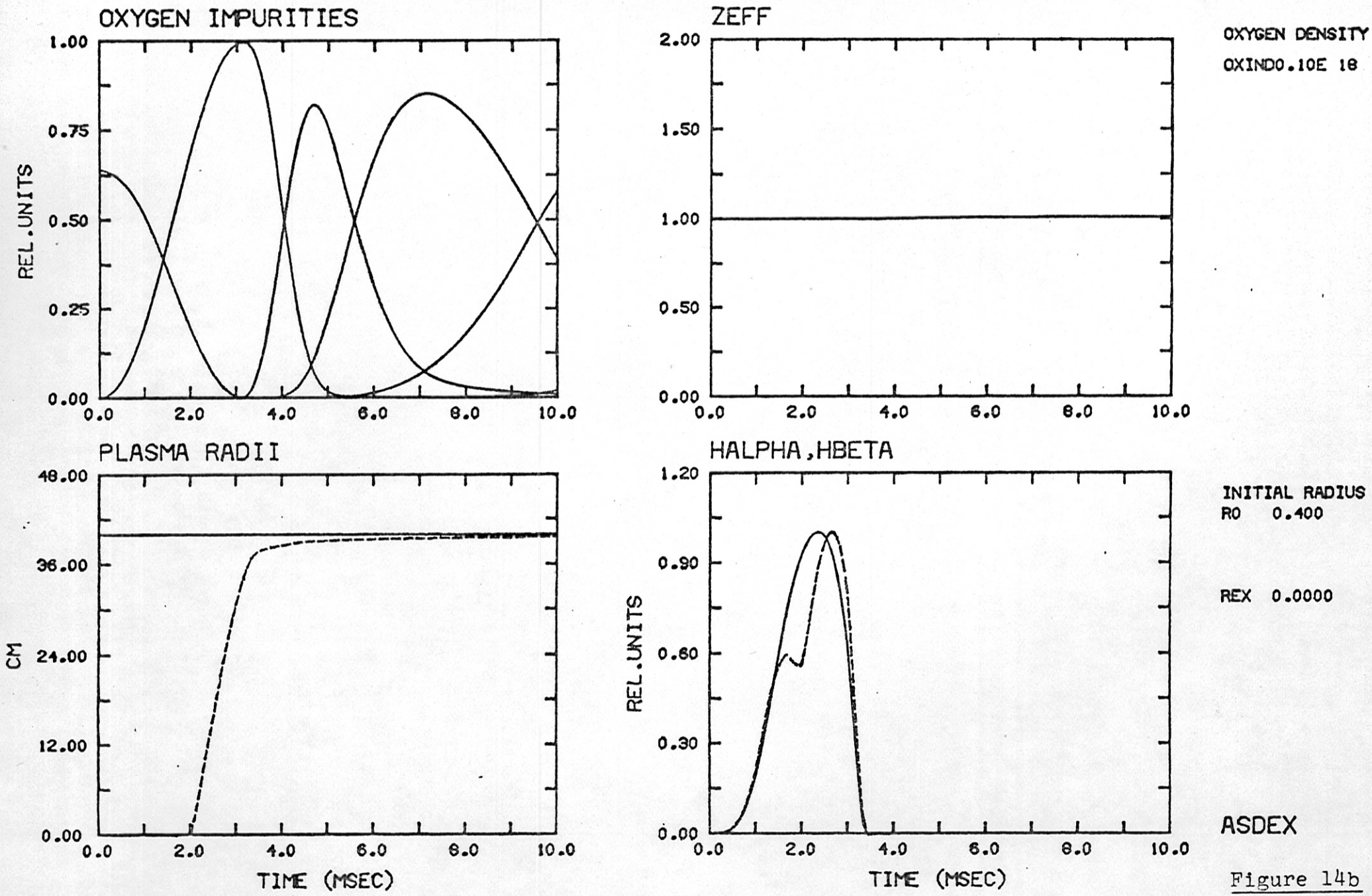

Figure 14b